12-2001

Current conduction through low angle grain boundaries in $YBa_2Cu_3O_{7-8}$ thin films studied magnetometrically

Hyunjeong Kim

To the Graduate Council:

I am submitting herewith a thesis written by Hyunjeong Kim entitled "Current conduction through low angle grain boundaries in $YBa_2Cu_3O_{7-\delta}$ thin films studied magnetometrically." I have examined the final electronic copy of this thesis for form and content and recommend that it be accepted in partial fulfillment of the requirements for the degree of Master of Science, with a major in Physics.

James R. Thompson, Major Professor

We have read this thesis and recommend its acceptance:

T. A. Callcott, D. G. Mandrus

Accepted for the Council:
Carolyn R. Hodges

Vice Provost and Dean of the Graduate School

(Original signatures are on file with official student records.)

...e Graduate Council:

I am submitting herewith a thesis written by Hyunjeong Kim entitled "Current Conduction through Low Angle Grain Boundaries in $YBa_2Cu_3O_{7-\delta}$ Thin Films Studied Magnetometrically." I have examined the final copy of this thesis for form and content and recommend that it be accepted in partial fulfillment of the requirements for the degree of Master of Science, with a major in Physics.

James R. Thompson

James R. Thompson, Major Professor

We have read this thesis

and recommend its acceptance:

T A Callcott

David R. Mandrus

Accepted for the Council:

Vice Provost and Dean of Graduate Studies

CURRENT CONDUCTION

THROUGH LOW ANGLE GRAIN BOUNDARIES

IN $YBa_2Cu_3O_{7-\delta}$ THIN FILMS

STUDIED MAGNETOMETRICALLY

A Thesis

Presented for

the Master of Science

Degree

The University of Tennessee, Knoxville

Hyunjeong Kim

December 2001

To every one who makes me stand here

ACKNOWLEDGMENT

First of all, my best thanks go to my adviser, Professor Dr. James R. Thompson, for everything making me accomplish this work. Without his help, encouragement, concern, and generosity, this work would not have been completed. I can never thank him enough. Thank you very much, Dr. Thompson!

I would like to extend my thanks to my parents and my brothers. Their endless support, encouragement, and trust make me stand here and keep my dreams.

I also would like to thank my committee members for their careful review and advice on this thesis. They are Prof. T. A. Callcott, and Prof. D. G. Mandrus.

Many thanks go to my colleagues at ORNL for their help. They are Dr. D. K. Christen, who projected and supported this work, Dr. H. R. Kerchner, Dr. D. T. Verebelyi, who did transport measurements, Dr. C. Cantoni, who made ring samples for this project, Dr. R. Feenstra, Dr. T. Aytug, K. Sorge, who helped me a lot with computer problems, Y. Zhang, N. F. Delene, and N. Ward.

Equal thanks go to my friends who never forget my being here and keep encouraging me from Korea. They are E. Y. Kim, S. K. Chin, H. B. Lee, S. H. Kim, J. I. Kim, S. H. Cho, H. J. Kim, and J. S. Kim. Especially, I would like to give special thanks to my roommate and fellow graduate student, H. I. Park who helped me a lot at a very important turning point in my life.

I also would like to express my thanks to Prof. C. Y. Lee and Prof. S. C. Ahn at Sejong University in Seoul, Korea. Their words of encouragement at Korea subsist in my mind as a big impulsive force.

ABSTRACT

Taking advantage of the sensitivity of SQUID-based instrumentation and a simple ring geometry that facilitates the calculation of a current in the sample, we introduce a new magnetometric method to obtain the critical current density flowing through grain boundaries in the high-temperature superconductor $YBa_2Cu_3O_{7-\delta}$ (YBCO). Since all magnetic moments originate from moving charges or electrical currents, an electrical current flowing in a simple configuration can be calculated from its magnetic moment or vice versa. Ring shaped YBCO films with or without [001]-tilt grain boundary were made on $SrTiO_3$ substrates on surfaces perpendicular to the **c**-axis. Magnetic moments of rings containing 1.8°, 2.8°, 5.1°, and 7° [001]-tilt grain boundaries were measured at various temperatures and fields parallel to the **c**-axis; as well, rings with no grain boundaries were measured for comparison. Current densities of the samples were calculated from the measured magnetic moments using a modified Bean critical state model. Especially, we could extract a pure grain boundary current density (current flowing across the grain boundary) from the total magnetic moment of a grain boundary ring. An abrupt decrease of the current density was observed as the grain boundary angle increased. Even small misorientations of $1.8^\circ < \theta \leq 5.1^\circ$ diminish the current density by a large amount, while a 1.8° grain boundary does not. Moreover, large peaks were found in curves of magnetic moment versus field for grain boundary samples under conditions of decreasing magnetic field (but not increasing field history). The appearance of a large peak in the $m(H)$ curves of a grain boundary sample can be explained by the weak-link

behavior of a small angle grain boundary. The high sensitivity of the magnetic moment and the grain boundary current density to field changes on a grain boundary strongly bolsters the weak-link interpretation of small angle grain boundaries.

CONTENTS

CHAPTER **PAGE**

1. INTRODUCTION 1

2. EXPERIMENTAL ASPECTS 6

2.1 SQUID Magnetometer 6

2.2 Sample Preparation 9

2.3 Experimental Studies 11

2.3.1 Temperature Sweep Experiments. 12

2.3.2 Field Sweep Experiments..... 13

2.3.2 Low Field Experiments..... 13

3. THEORETICAL BACKGROUND 14

3.1 YBCO ($YBa_2Cu_3O_{7-\delta}$, where $0 < \delta < 0.6$) 14

3.2 Pairing Symmetry 17

3.3 The Vortex State 20

3.4 Bean Critical State Model 24

3.5 The Josephson Junction 27

3.6 Grain Boundaries. 30

4. EXPERIMENTAL RESULT AND DISCUSSION..... 33

4.1 Analytical methods. 33

4.2 Results of Temperature Sweep Experiments. 41

4.3 Results of Field Sweep Experiments. 49

4.4 Results of Low Field Study. 59

4.5 Discussion. 64

5. CONCLUSIONS..... 70

REFERENCES..... 73

VITA..... 76

List of Figures

2-1 The system components of the SQUID magnetometer of Quantum Design's MPMS-7. 7

2-2 The configuration and location of the pickup coils. 8

2-3 Making ring samples; (a) A substrate with a grain boundary, (b) A deposited YBCO film, (c) Etching off a film to make the form of a ring, and (d) Cutting a film in three pieces. 10

3-1 The structure of $YBa_2Cu_3O_7$. G. Burns, "High-Tempsrature Superconductivity," Academic Press, Inc. (1992). 15

3-2 Electron pairing in s- and d- wave superconductors. (a) Conventional s-wave (l=0) Pairing, and (b) Novel d-wave (l=2) pairing. 19

3-3 The internal structure of an isolated flux line; λ is the penetration depth and ξ is the coherence length. 21

3-4 Magnetic phase diagrams for (a) a conventional superconductor and (b) for high-T_c superconductor. 23

3-5 The magnetic field profile inside a superconductor and the magnetization curve with pinning. (a) in increasing field and (b) in decreasing field. V. Z. Kresin and S. A. Wolf, "*Fundamentals of Superconductivity*," Plenum Press, New York (1990). 26

3-6 Josephson current as a function of magnetic field. V. Z. Kresin and S. A. Wolf, "*Fundamentals of Superconductivity*," Plenum

Press, New York (1990). 29

4-1 Current flow in samples with various geometries. (a) a current loop, (b) a ring Sample, and (c) a rectangular sample. 34

4-2 Current configurations: (a) ring-like current flow and (b) strip-like current flow. 37

4-3 Detailed current flow near a grain boundary. 39

4-4 A comparison of 1.8° grain and open rings: (a) magnetic moment versus temperature, and (b) current density versus temperature. 42

4-5 Current density versus temperature at 5 K for a GB and its companion grain ring. (a) 1.8°, (b) 2.8°, (c) 5.1°, and (d) 7° samples. 43

4-6 Grain boundary current density versus temperature plotted in logarithmic scale. 45

4-7 GB current density (normalized) versus misorientation angle. (a) normal scale, and (b) logarithmic scale. 47

4-8 Strip-like moment versus temperature. 48

4-9 Magnetic moment versus field at 5 K. (a) 5.1° grain ring and (b) 1.8° open ring. 50

4-10 Current density versus field for 5.1° grain and 1.8° open rings at 5 K. (a) normal scale and (b) logarithmic scale. 51

4-11 Field dependent magnetic moment and current density of 1.8° GB and companion grain ring samples at 5 K. (a) magnetic moment versus field, and (b) current density versus field. 53

4-12 $m(H)$ curves of 5.1° and 7° GB rings comparing with those grain and open rings

at 5 K, (a) with 1.8° open ring and (b) with 5.1° grain ring. 54

4-13 m(H) curves of a 2.8° GB ring, compared with those of companion grain and 5.1° GB rings at 5 K. (a) with companion grain ring and (b) with 5.1° GB ring. 56

4-14 H_{peak} and $J_c^{Gr}(H_{peak})$ versus temperature for 2.8°, 5.1°, and 7° GB rings. (a) H_{peak} and (b) $J_c^{Gr}(H_{peak})$. 57

4-15 Peak field versus corresponding companion grain current density. 60

4-16 Magnetic moment versus field in the low field range: (a) grain, 2.8°, 5.1°, and 7° GB rings, and (b) open, 5.1°, and 7° GB rings. 61

4-17 Magnetic moments at 5 K, showing in-field and trapped flux values, (a) for 2.8° and 5.1° GB ring. The symbols (×) and (▲) are values measured in H=0; they are plotted at values of H at which flux was trapped and (b) for a grain ring. 63

4-18 Magnetic moment versus field in the low field range for a 5.1° GB ring at various temperatures. 65

4-19 Magnetic moment changes due to applied field changes for a 5.1° GB ring at 5 K; sudden decrease of an applied field from 2.2 kOe and 4kOe during increasing field history (asterisks for 2.2 kOe and triangles for 4 kOe) and sudden increase of an applied field from 4 kOe, 2.6 kOe and 1.8 kOe during decreasing field history (diamonds for 4 kOe, circles for 2.6 kOe, and squares for 1.8 kOe). 69

CHAPTER 1

INTRODUCTION

When some materials are cooled to a sufficiently low temperature, their electrical resistivity suddenly drops to zero at a temperature called the critical temperature, T_c. The phenomenon is called superconductivity and was first discovered in mercury by K.Onnes in 1911. In the superconducting state, an ideal material also exhibits the property of perfect diamagnetism when it is immersed in a weak magnetic field. This means that applied magnetic fields are completely expelled from the body of a superconductor. This perfect diamagnetic property seems to be easily explained by an induced current that is the result of changes of the applied field. However, when a normal state superconductor in a static magnetic field is cooled down below T_c, the applied magnetic field is expelled from a superconductor even though there are no changes in the applied field to create induced currents (Meissner effect). Those two features, zero resistivity and the Meissner effect, are major characteristics of superconductors.

Many brilliant physicists worked to find an explanation for these fascinating phenomena. The London theory and Ginzburg-Landau theory succeeded in explaining macroscopic properties of a superconductor while the BCS theory provides a microscopic explanation.

When a conductive material is brought to a sufficiently low temperature, thermally excited electrons on the Fermi surface lose some of their energies so that they slow down slightly. According to the BCS theory, in the superconducting state, among

those electrons, two electrons that have opposite velocities (v and $-v$) and opposite spins attract each other and become a Cooper pair which conducts a supercurrent. The size of a Cooper pair is called the coherence length, ξ. This electron coupling is due to the lattice vibrations, or phonons. The interaction of two electrons is mediated by an attractive force that positively charged ions of the lattice exert on each electron.[1]

Because two electrons with opposite velocity create a Cooper pair, the velocity of a Cooper pair is zero and according to de Broglie's relation, $\lambda = h/mv$ the wavelength of a Cooper pair is infinitely long. This means that the phase of a Cooper pair-wave does not change spatially inside a superconductor. Moreover, Cooper pairs are Bose particles because their spins are zero and therefore all of them can occupy a single energy state.[2]

According to the theory of wave propagation in discrete structures, when a wave passes through a periodic lattice, it continues propagating indefinitely without scattering, i.e. without modification in either direction or intensity.[3] Since an electron can be treated as a matter wave, the conduction electron should not be scattered by a regular lattice of ions at all. Electrical resistance arises because of the deviation of the lattice from perfect periodicity such as lattice vibration and presence of impurities and dislocations.[3] In theory, therefore, a perfectly crystalline conductor should offer no resistance. R. de Picciotto and his colleagues' recent study has shown that this is actually true.[4] For the case of superconductors, zero resistance occurs not because of perfect crystals but because of the existence of an energy gap at the Fermi surface, between filled and empty states. Under an attractive interaction between two electrons, the system of two electrons is in bound state forming an energy gap between two energy levels. In the superconducting state, where two electrons pair up, a gap is formed at the Fermi surface

with width 2Δ. Since the superconducting phenomenon usually occurs at low temperatures, the scattering of a single electron by phonons is negligible, because the amplitudes of oscillation are very small and hence the scattering by impurities is usually predominant. Due to the energy gap, small amounts of impurities can not scatter Cooper pair-waves; a Cooper pair is not broken because it needs more energy to break up than to keep a Cooper pair when it meets impurities. This is the reason why materials in the superconducting state have zero resistivities.

As soon as a sample in an applied static magnetic field is cooled below its critical temperature, T_c, magnetic field lines are expelled from the superconductor, *except* in the surface layer of the superconductor. The depth of penetration in the surface layer is called the penetration depth, λ. Because a magnetic field penetrates a distance λ, the vector potential A also extends over a length λ. This vector potential causes changes of the phase distributions of Cooper pair-waves with an amount $k=(2\pi q/h)A$. In order for the superconducting state to exist, the phases of Cooper pair-waves must be constant everywhere inside a superconductor. To prevent the vector potential from transmuting the phase distributions of Cooper pair-waves, supercurrents (i.e. flows of Cooper pairs) begin to flow in such a way that the phase changes due to the supercurrents can compensate the phase change due to the vector potential : spatial phase changes of Cooper pair-waves caused by supercurrents completely cancel the changes induced by the vector potential in the surface layer of a superconductor. This flow of Cooper pairs creates magnetic fields in an opposite direction of the applied field and the magnetic field inside a superconductor becomes zero.

Superconductors can be divided in two major groups, type-I and type-II, according to their response to a magnetic field. The type-I superconductors exclude applied magnetic fields completely from their bodies up to a critical field, H_c , which destroys superconductivity. However, for type-II superconductors, instead of breaking down the superconducting state, quantized magnetic flux lines begin to penetrate the superconductors as thin filaments called vortices. This procss begins at a lower critical field H_{c1}. This state, the vortex state or mixed state, continues up to an upper critical field H_{c2} where the superconducting state reverts to the normal state.

In 1986, J. G. Bednorz and K. A. Muller's discovery of superconductivity in $(La\text{-}Ba)_2CuO_4$ opened the era of high-temperature superconductors (HTS) with T_c above the temperature of liquid-nitrogen (77K) ; an Y-based family with T_c up to 90K, a Bi-based family with T_c up to 110K, a Tl-based family with T_c up to 125K, and a Hg-based family with T_c up to 133K.[5] All of these high-temperature superconductors are type-II superconductors and contain CuO_2 planes where supercurrents flow.

Those high-T_c superconductors have major problems in making resistance-free wires. First of all, they are ceramics, which are brittle and not flexible. Second, the movement of vortices generates heat and causes current conduction to be dissipative. Finally, the high-temperature superconductors have highly anisotropic properties which contribute to a significant reduction of the critical current density across grain boundaries. Solutions for those problems have been suggested and examined. For the solution of the second problem, the idea of confining vortices in defects was suggested. Columnar defects formed by heavy-ion irradiation, and splayed columnar defects induced by high-energy proton irradiation have succeeded in greatly increasing the critical current

density J_c at high magnetic fields. As far as the first and the third problem is conceived, the method of growing HTS layers on some flexible substrates has been widely studied. Especially, a recently developed technique, Rolling-Assisted Biaxially Textured Substrate (RABiTS) reduces the degree of grain boundaries from high angles to low angles. Nevertheless, even low angle grain boundaries play an important role in reducing the critical current density J_c of high-temperature superconductors. Therefore, a thorough study of grain boundaries is necessary to develop efficient superconducting wires.

The present investigation is directed to the properties of low angle grain boundaries on single crystal YBCO thin films, elicited from magnetic measurement studies. Chapter 2 gives a brief description of the main experimental aspects such as SQUID, sample preparation, and sequences for the measurements. Chapter 3 gives the theoretical background required for an analysis of the experimental data, general properties of YBCO, and other grain boundary related studies. The experimental results and analysis is followed by the conclusion.

CHAPTER 2

EXPERIMENTAL ASPECTS

2.1 SQUID Magnetometer[5]

Magnetic studies were conducted in a SQUID (Superconducting Quantum Interference Device)-based magnetometer, Quantum Design model MPMS-7. Quantum Design's Magnetic Property Measurement System (MPMS) is a highly integrated instrument system. The model MPMS sample magnetometer is designed to detect the magnetic moment of a sample. Figure 2-1 shows the system components. The fully automated temperature control system can vary the temperature from 2 K (-271 °C) to 400 K (127 °C). A high homogeneity superconductive magnet provides magnetic fields up to ±7 T. It is energized with current from a power supply. A measurement is performed in the MPMS system by moving a sample through the superconducting detection (pickup) coils (Figure 2-2). The longitudinal pickup coils consist of a highly balanced second-derivative coil set. The upper coil is a single turn wound clockwise, the center coil comprises two turns wound counter-clockwise, and the bottom coil is a single turn wound clockwise so that noise can be countervailed. When the sample moves through the pickup coils, the magnetic moment of the sample induces an electric current in the pickup coils. Since pickup coils, connecting wires, and SQUID input coils form a closed superconducting loop, any change of magnetic flux in the pickup coils produces a

SYSTEM COMPONENTS

1. Sample Rod
2. Sample Rotator
3. Sample Transport
4. Probe Assembly
5. Helium Level Sensor
6. Superconducting Solenoid
7. Flow Impedance
8. SQUID Capsule with Magnetic Shield
9. Superconducting Pick-up Coil
10. Dewar Isolation Cabinet
11. Dewar
12. HP Thinkjet Printer
13. Magnet Power Supply
14. Model 1802 Temperature Controller
15. Console Cabinet
16. Power Distribution Unit
17. Model 1822 MPMS Controller
18. Gas/Magnet Control Unit
19. HP Vectra Computer
20. Monitor

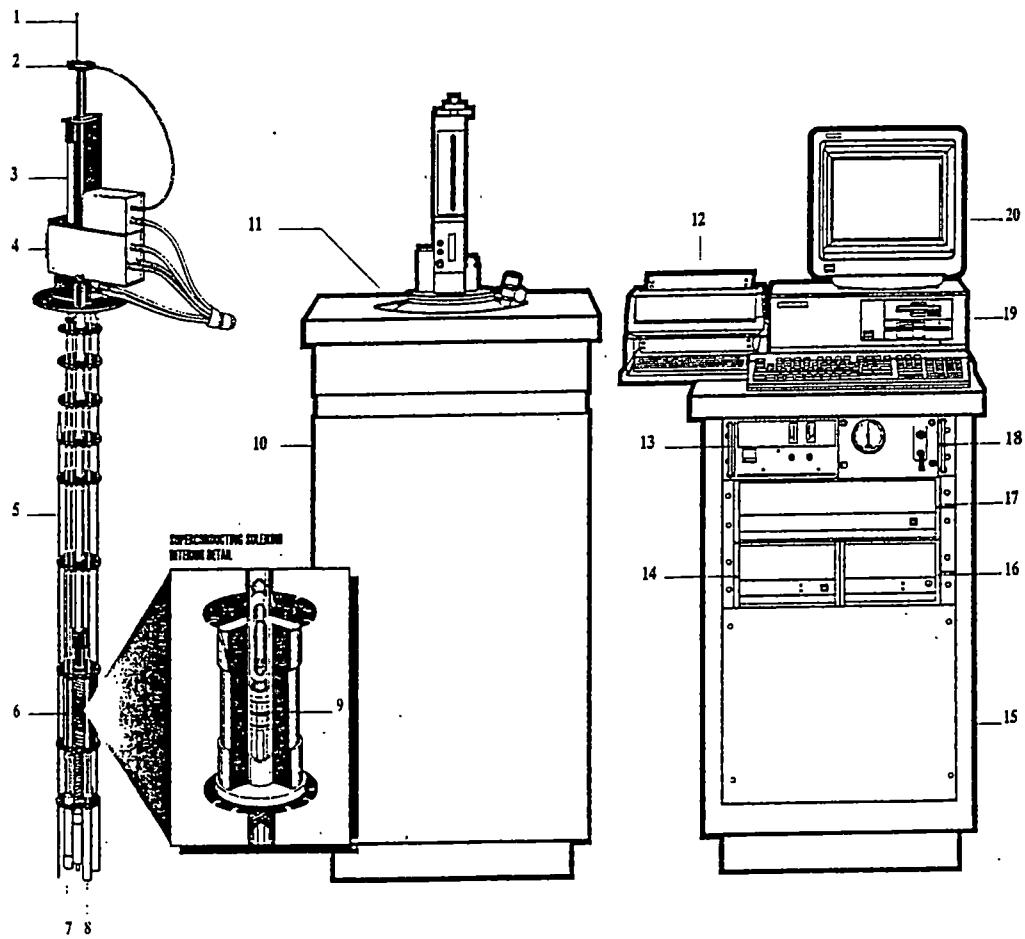

Figure 2-1. The system components of the SQUID magnetometer of Quantum Design's MPMS-7.

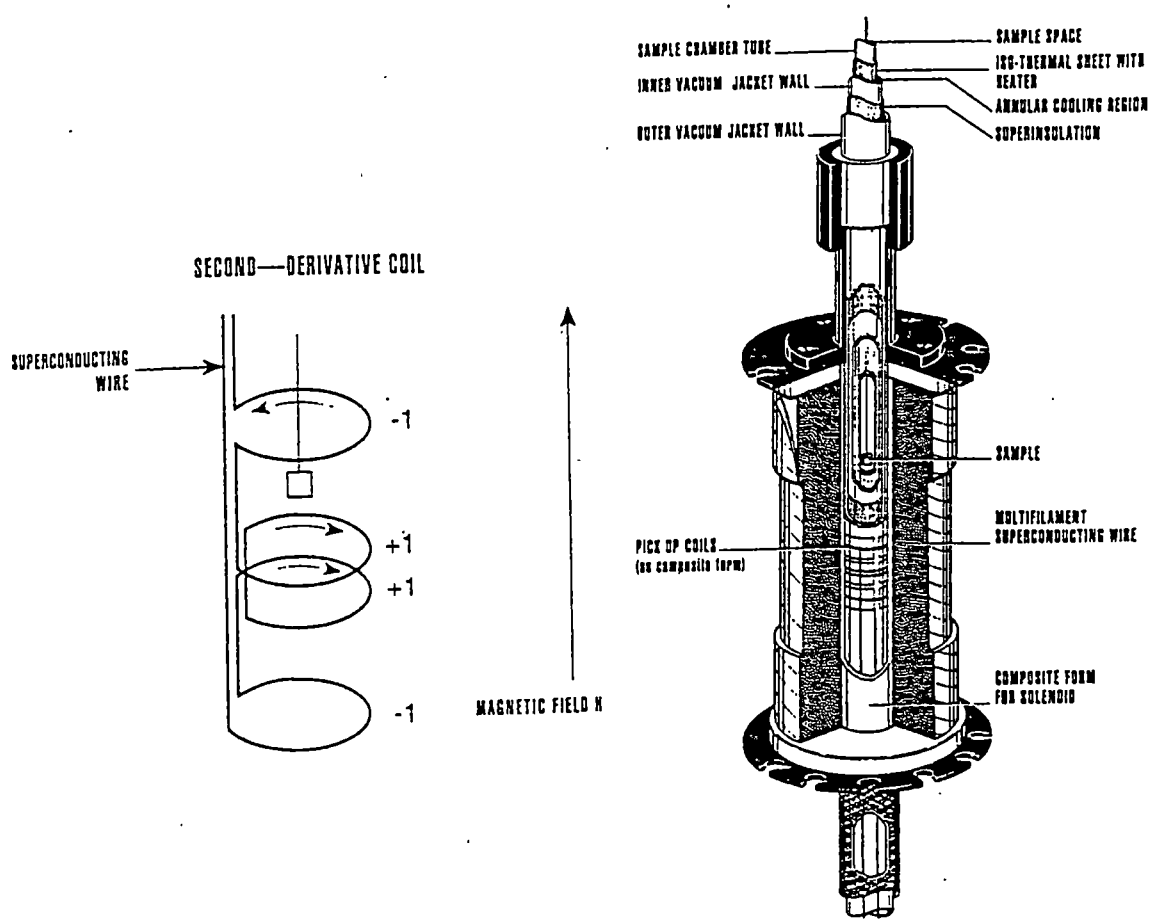

Figure 2-2. The configuration and location of the pickup coils.

change in the persistent current in the pickup detection circuit, which is proportional to the change in magnetic flux. Because the SQUID functions as a highly linear current-to-voltage convertor, the variations in the current in the pickup coils produce corresponding variations in the SQUID output voltage which is proportional to the magnetic moment of the sample.

The MPMS can measure a magnetic moment with a range of sensitivity from about 10^{-7} emu to 2 emu in the standard configuration and can measure over 300 emu with the extended range option. Usually, the MPMS reports the magnetic moment data in emu (electromagnetic units [$G \cdot cm^3$]).

2.2 Sample Preparation

Films of YBCO were prepared on $SrTiO_3$ (STO) [001]-tilt bicrystal substrates by the pulsed laser deposition method (Figure 2-3-a and b). Three ring samples were made on each YBCO film by ordinary optical photolithography techniques (Figure 2-3-c). One ring was placed across a grain boundary in order to make a ring with two grain boundaries (GB ring) and two other rings were patterned on each of the two adjoining single crystals (grain rings). All three rings have the same geometry with an outside diameter of 3 mm, a width of 100 μm, and a thickness of 200 nm. Each substrate was cut into three pieces, each containing just one ring (Figure 2-3-d). It must be noticed that all the three rings are from one YBCO film and as a result, they have the same film properties such as current density, pinning force, etc. Bicrystal substrates with 1.8°, 2.8°,

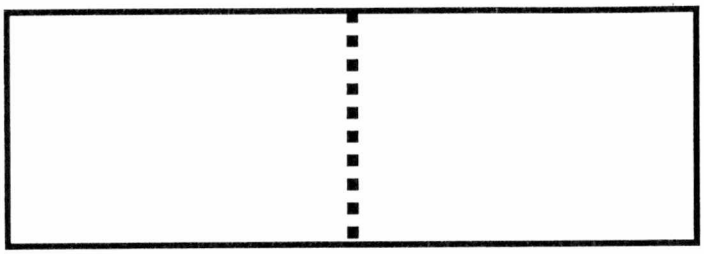

(a) A substrate with a grain boundary.

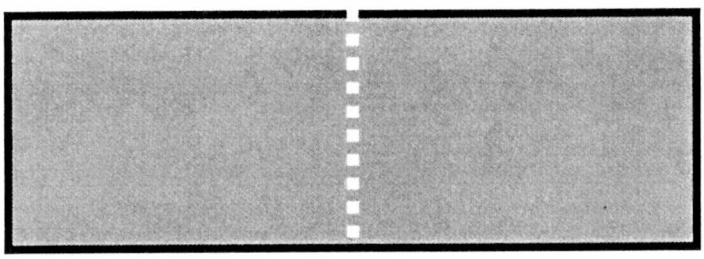

(b) A deposited YBCO film.

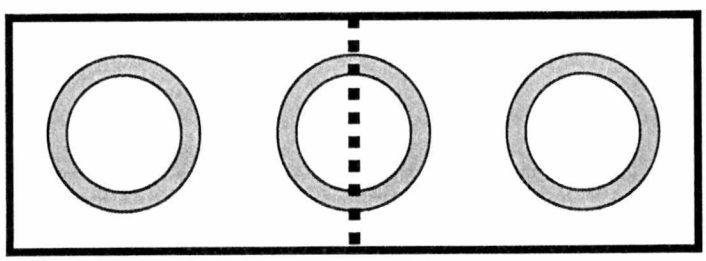

(c) Etching off a film to make the form of a ring.

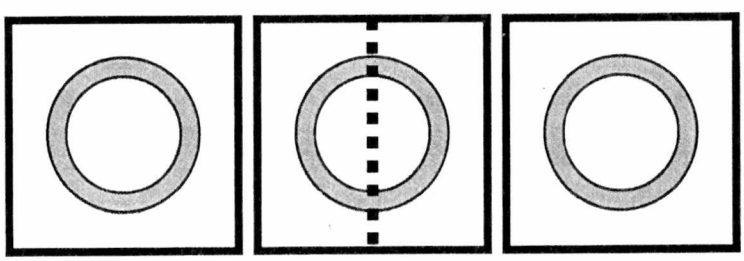

(d) Cutting a film in three pieces.

Figure 2-3. Making ring samples.

5.1°, and 7° [001]-tilt boundaries were used to make GB and companion grain ring samples.

Sometimes the current density can be diminished by external degrading factors, such as cracks on a sample or by maltreatment. In order to be convinced of measured current density values of grain rings, some grain rings were made into an open circuit by etching a line across the 100 μm width (open rings). This changes the geometry of the current path without changing the properties of the superconductor. An individual sample was mounted on a Si disk with Duco cement and placed in a Mylar tube for support during magnetic measurements.

2.3 Experimental Studies

A circulating charge or current causes a magnetic dipole moment according to the equation in CGS unit,

$$\vec{m} = \frac{1}{2 \cdot c} \int (\vec{r} \times \vec{J}(\vec{r})) \cdot d\tau \qquad (2\text{-}1)$$

where $\vec{m}$ is the magnetic dipole moment, $\vec{J}(\vec{r}) \cdot d\tau$ is an element of current, and c is the speed of light. According to equation (2-1), once the configuration of a current flow is known, currents or current densities can be calculated from measured magnetic moment values of the sample. The configuration of a current flow is related to the sample geometry. If a sample has symmetry in its geometry and its current density is constant spatially inside the sample, then the integral in equation (2-1) can be calculated very easily. For the case of a ring sample, the configuration of a current flow is

circumferential. In the Meissner state, the circulating currents are induced in the surface layer of a superconductor with width equal to the penetration depth, λ. In the vortex state, circulating currents due to the distribution of vortices are induced and flow in the entire sample after the applied field exceeds the field of full penetration. With this idea, the interval of an integral can be determined for each case. Values measured by a SQUID magnetometer are the magnetic moments produced from those circulating currents and they can be very accurate due to the sensitivity of SQUID. Using this experimental set-up, responses of current densities to various circumstances, such as at different fields and temperatures, can be observed.

The ring study consists of two major parts. For each ring, the magnetic moment was measured as a function of temperature (the temperature sweep experiment) and magnetic field (the field sweep experiment). To study the low field dependent behavior of a grain boundary in more detail, some field sweep experiments were repeated with finer steps.

2.3.1 Temperature Sweep Experiments

The rings were first located at the center of the pick-up coils in the magnetometer at 5 K, whose magnet was reset earlier to release trapped flux in its windings. Then a sufficiently large external magnetic field was applied parallel to the **c**-axes of the YBCO ring films, so that samples were fully penetrated by the fields. Those applied fields were 500 Oe, 3 kOe, and 500 Oe for Grain, GB, and open rings respectively. After removing applied fields to obtain maximum induced magnetic moments that samples could have at

5K, the magnetic moments were measured while increasing temperatures from 5 K to 95 K in 1K steps.

2.3.2 Field Sweep Experiments

After temperature sweep experiments, the magnet of the magnetometer was reset. Samples were made virgin by setting the temperature above T_c and then superconductive again by decreasing temperature down to 5 K. Field-dependent moments were measured while increasing applied magnetic fields from 0 Oe to 65 kOe and then decreasing from 65 kOe to 0 Oe. The magnetic fields were applied perpendicular to the **ab**-plane of YBCO film. This field sweep sequence was run for eavh ring at temperatures, 5, 10, 20, 40, 60, 77, and 85 K. Before running the field sweep sequence at each temperature, samples were always made virgin by setting the temperature above T_c.

2.3.3 Low Field Experiments

For a closer study of the field-dependence of the grain boundary behavior, the moments of all the samples, GB, grain, and open rings, were measured at 5 K with gradually increasing field up to 100 Oe in fine steps.

CHAPTER 3

THEORETICAL BACKGROUND

3.1 YBCO ($YBa_2Cu_3O_{7-\delta}$, where $0 < \delta < 0.6$)

In 1986, J. Georg Bednorz and K. Alex Müller were pursuing the idea that higher T_c values might be found in materials in which the Jahn-Teller effect could enhance the electron-phonon coupling parameter.[6] After years of effort, they discovered a superconducting material with T_c in excess of 30 K. The new material was based on La_2CuO_4, which is an insulator. In this system, ions of Ba^{2+}, Sr^{2+}, or Ca^{2+} replace some of the La^{3+} (hole doping). High-temperature superconductors, like $La_{2-x}Sr_xCuO_4$, are obtained by adding charge carriers to a Mott insulator.

One of the most thoroughly studied superconductors, YBCO ($YBa_2Cu_3O_{7-\delta}$), with $T_c \approx 92$ K, was discovered in early 1987 (Figure 3-1). Like other high-temperature superconductors, YBCO has Cu-O planes perpendicular to the **c**-axis. The superconductivity and charge transport are mostly confined to the Cu-O planes. Two immediately adjacent Cu-O planes, about 3.2 Å apart, are separated from each other by a single Y-atom plane. In YBCO, a pair of two immediately adjacent Cu-O planes is approximately 8.2 Å apart from the next pair. Between one pair of immediately adjacent Cu-O planes and the next pair, three metal-O planes are found. In one of those three

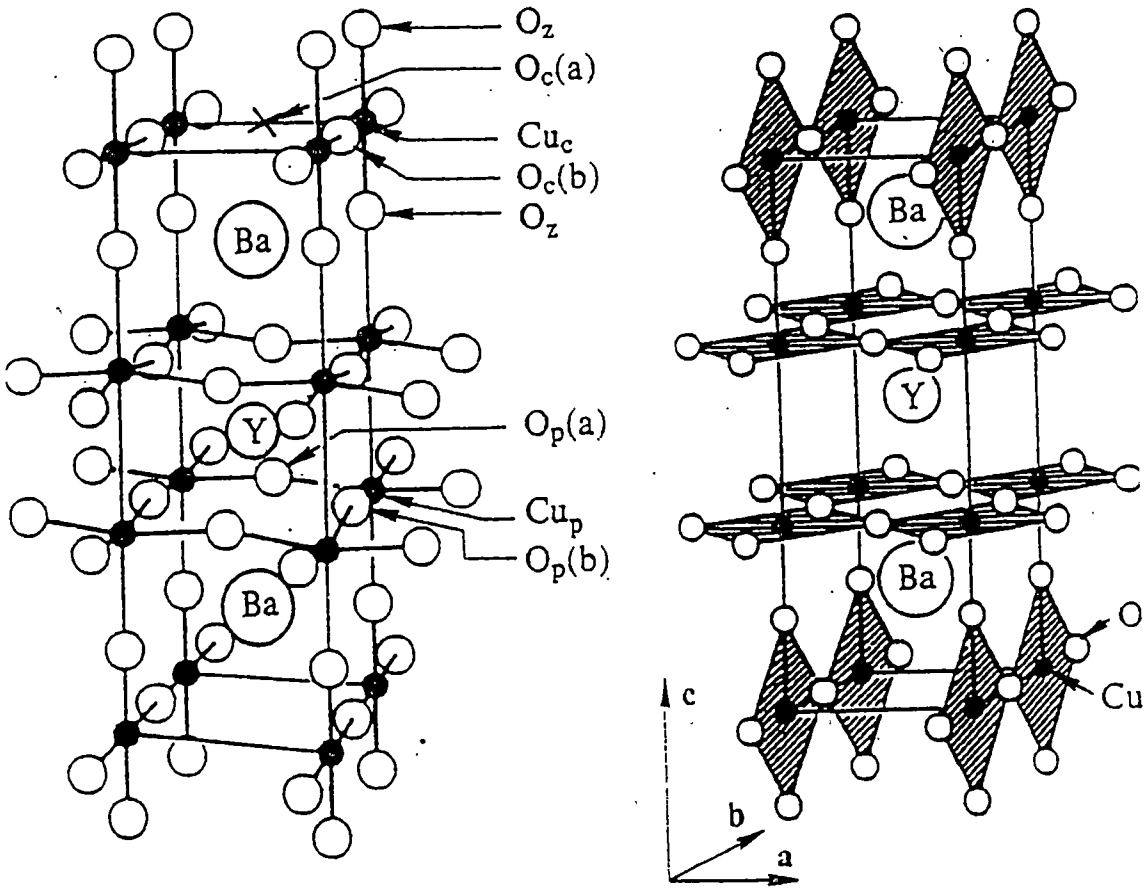

Figure 3-1. The structure of $YBa_2Cu_3O_7$. G. Burns, *"High-Temperature superconductivity,"* Academic Press, Inc. (1992)

layers, Cu and O atoms form Cu-O chains. These Cu-O chains are referred to as "charge reservoirs." In both Cu-O planes and chains, Cu atoms are strongly covalently bonded to four O atoms in a square-planar configuration.[6] However, the Cu-O planes extend indefinitely in two directions (the **ab**-plane), while the Cu-O chains extend indefinitely in only one direction (the **b**-axis).

Like other high-temperature superconductors, superconducting YBCO can be obtained by adding more oxygen to a parent Mott insulator, $YBa_2Cu_3O_6$ (hole doping). The Cu-O planes in $YBa_2Cu_3O_6$, remain the same as in YBCO but the chains contain linear, two-coordinated Cu atoms in O-Cu-O "sticks;" The only oxygen atoms in Cu-O chains are the ones located along **c**-axis in the $YBa_2Cu_3O_6$ system. These O-Cu-O sticks contribute to the tetragonal structure of $YBa_2Cu_3O_6$. When extra oxygen atoms are introduced to $YBa_2Cu_3O_6$, they begin occupying the Cu-O chains, changing the structure from tetragonal $YBa_2Cu_3O_6$ to orthorhombic $YBa_2Cu_3O_{7-\delta}$. Electron diffraction studies on carefully prepared samples with intermediate oxygen content (between O_6 and O_7) reveal a variety of superstructures with different repeats along the a-axis due to the oxygen occupation.[6]

The superconducting state appears at $\delta \leq 0.6$, when the oxygen content exceeds about 6.4 ($YBa_2Cu_3O_{6.4}$). Below $\delta = 0.6$, holes are transferred from the Cu-O chain to the Cu-O plane, which immediately destroys the normal antiferromagnetic order and is accompanied by metallization.[7] In the region $0.3 \leq \delta \leq 0.6$, the hole concentration in the Cu-O plane is kept low with relatively low superconducting transition temperature $T_c \sim$ 60 K. Around $\delta = 0.3$ the hole concentration is increased quickly to the optimally doped or overdoped region with $T_c \sim 90$ K.[7]

3.2 Pairing Symmetry

The symmetry of the order parameter is basically a question of the internal structure of the Cooper pair in the high-temperature superconductors. It is well known that superconductivity arises from the formation of electron pairs that condense into a coherent macroscopic quantum state. The essence of the pairing symmetry can be considering the structure of the quantum mechanical wave function of a single pair.[8]

Let the wave functions of the two electrons of a Cooper pair be $\phi_k(\vec{r}_1, s_1)$ and $\phi_{k'}(\vec{r}_2, s_2)$, where $\vec{r}$ represents the spatial coordinates of the particle and s represents the spin. If these electrons form a Cooper pair, then the pair function will have the form:

$$\Psi(\vec{r}_1, s_1; \vec{r}_2, s_2) = \Psi(\vec{R})\Phi(\vec{\rho})\chi(s_1, s_2)$$

where $\vec{R} = (\vec{r}_1 + \vec{r}_2)/2$ is the coordinate of the center of mass, $\vec{\rho} = (\vec{r}_1 - \vec{r}_2)$ is the relative coordinate, and $\Psi(\vec{R})$, $\Phi(\vec{\rho})$, and $\chi(s_1, s_2)$ describe the center of mass, the internal structure, and the spin of the Cooper pair, respectively.[9] The macroscopic properties of a superconductor, such as zero resistance, the Meissner effect, and the flux quantization, depend on $\Psi(\vec{R})$ which is the well-known Ginzburg Landau order parameter. The microscopic properties of a superconductor, such as the energy gap and detailed temperature dependence, depend on $\Phi(\vec{\rho})$.[8] The wave function of the internal structure of the pair can be written as a linear combination of spherical harmonics $Y_{lm}(\theta, \varphi)$ multiplied with a radial function $R(\rho)$, where ρ is the separation of the particles:

$$\Phi(\vec{\rho}) = \sum_{lm} c_{lm} Y_{lm}(\theta, \varphi) R(\rho)$$

The total spin wave function, $\chi(s_1, s_2)$, is either a spin triplet (total spin $s = 1$) with symmetric spin wave function, or a spin singlet (total spin $s = 0$) with antisymmetric spin wave function. For a pair of fermions, the total wave function, $\Psi(\vec{r}_1, s_1; \vec{r}_2, s_2)$, should be antisymmetric when the two particles are exchanged. Thus, for the spin-singlet wave function ($s = 0$), the orbital part of the total wave function, $Y_{lm}(\theta, \varphi)$ must be symmetric and have s-state ($l = 0$), d-state ($l = 2$), ... orbital angular momentum. Similarly, the spin-triplet ($s = 1$) must have p-state ($l = 1$), f-state ($l = 3$), ... orbital angular momentum.

In a conventional superconductor, a Cooper pair is formed by electrons with opposite spins and momentum, i.e. spin singlet with s-state orbital angular momentum (Figure 3-2-a).[8]

It has been found that the high-temperature superconductor has d-wave pairing symmetry. For the d-wave case, two electrons of a Cooper pair can be thought of as in counter circulating orbits (Figure 3-2-b).[8] The wave function of d-wave symmetry changes sign and has nodes and antinodes as one goes around the origin. Furthermore, the existence of nodes for a d-wave superconductor means that there are always normal electrons in the system at low energies near the Fermi surface. Furthermore, the density of states depends on the angle from the **a**-and **b**-axes of Cu-O planes in the high temperature superconductors.

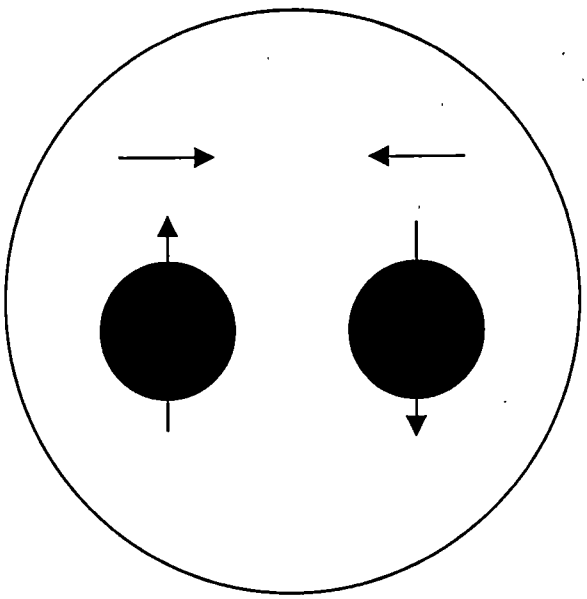

(a) Conventional s-wave (l=0) pairing

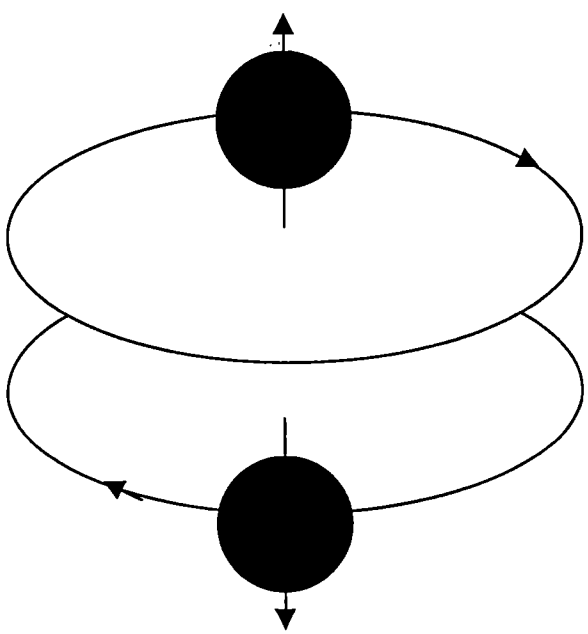

(b) Novel d-wave (l=2) pairing

Figure 3-2. Electron pairings in s- and d-wave superconductors.

3.3 The Vortex State

All high-temperature superconductors are, as mentioned previously, type II superconductors. For a type II superconductor, the magnetic field begins to penetrate into the sample forming a vortex (a quantized flux line) when the applied magnetic field reaches the lower critical field, H_{c1}. The superconductor then enters the mixed state or vortex state. This occurs because the energy cost is reduced, if fields are allowed to partially penetrate the superconductor. In 1957, A. A. Abrikosov theoretically predicted that when the Ginzburg-Landau parameter κ (the magnetic penetration depth divided by the coherence length $\kappa \equiv \lambda/\xi$) is larger than $1/\sqrt{2}$ ($\kappa > 1/\sqrt{2}$), a vortex state can be formed. As soon as the magnetic field begins to penetrate into a sample at H_{c1}, because of the influence of the Lorentz force, a fraction of electrons begin to move in a circle. This results in the appearance of vortices in the superconductor. The superconducting electrons circulate around the axis of the vortex. These circulating currents are not transport currents but rather a localized supercurrent. Closer to the vortex axis, the electrons revolve faster. At some distance from the axis, the speed exceeds a critical value and superconductivity is depressed, i.e. the superconducting order parameter reaches zero.[10] Therefore, the core of the vortex, whose radius is approximately equal to a superconducting coherence length ξ (typically 10~20 $\AA$ in high temperature superconductors at low temperatures) is in the normal state.[11] More properly, the superconducting order parameter is depressed. Inside a vortex, the magnetic field is nonzero, and every vortex line has one magnetic flux quantum, $\Phi_0 = h/2e$ (Figure 3-3).

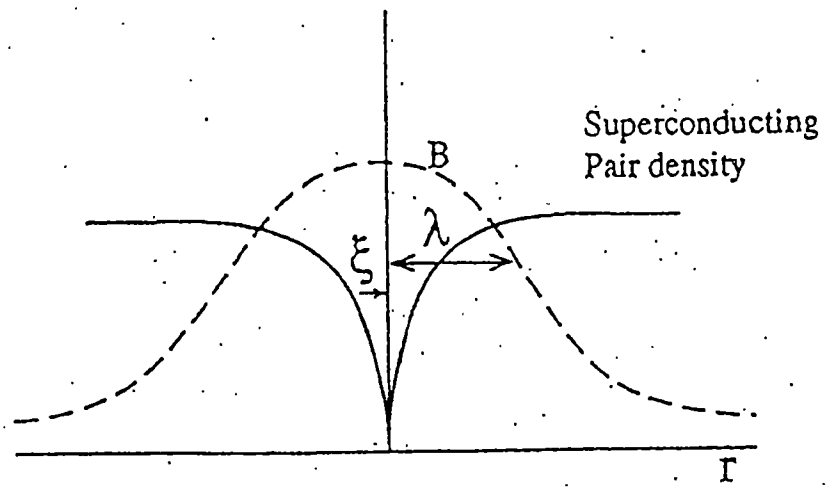

Figure 3-3. The internal structure of an isolated flux line; λ is the penetration depth and ξ is the coherence length.

As the external magnetic field is increased, vortices are pushed closer together and the interaction between vortices becomes stronger until the upper critical field H_{c2} is reached. The interaction is repulsive: for an isotropic interaction, vortices form a triangular lattice whose structure gives the greatest separation of nearest neighbors, and therefore the interaction energy is minimum in this vortex array. In this array, the nearest neighbor distance is

$$a = \left(\frac{4}{3}\right)^{1/4} \cdot \left(\frac{\Phi_0}{B}\right)^{1/2} = 1.075 \cdot \left(\frac{\Phi_0}{B}\right)^{1/2}.$$

It is important that in the space between the vortices the material remains superconducting. This is where a transport electric current flows.

A vortex interacts not only with other vortices but also with defects in a sample. Defects in high-temperature superconductors can be dislocations, twins, oxygen nonstoichiometry, or other atomic defects.[11] Those defects pin vortices on their sites. Using this idea, defects whose radii approximately match the coherence length were artificially created to trap vortices, in order to obtain high bulk current densities. Because the defects are randomly distributed in a sample, this vortex pinning by defects breaks the ideal triangular vortex lattice. Therefore, there is no long-range spatial order in this vortex state. This state is known as the vortex-glass state. Figure 3-4 shows the *H-T* phase diagram for a high-temperature superconductor. Either thermal excitations or quantum tunneling can cause vortices to escape from their pinning sites and move in the direction of the Lorentz force, which lowers the current density of the sample.

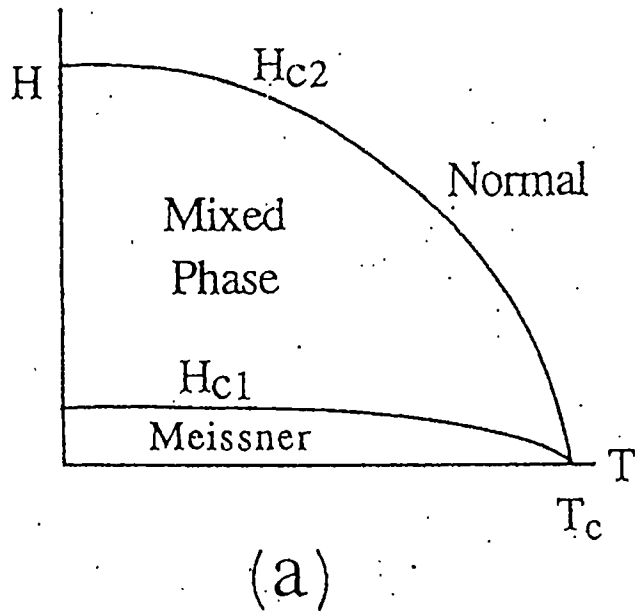

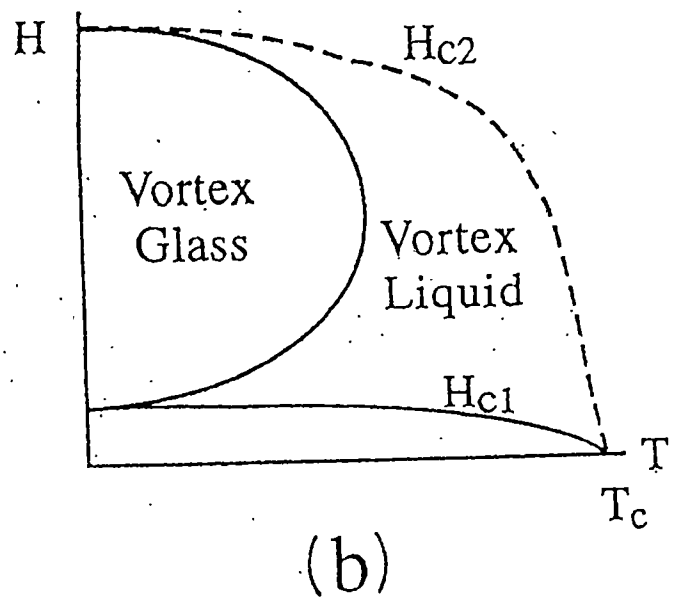

Figure 3-4. Magnetic phase diagrams for (a) a conventional superconductor and (b) for high-*Tc* superconductor.

3.4 Bean Critical State Model

Often one needs to estimate the critical current density of a sample on which it is difficult to perform a direct transport measurement, for example, a small single crystal. In this case, the critical current density can be estimated from a magnetization measurement by utilizing the hysteresis in the magnetization curves. The model that is usually used is the critical state model, which was introduced by C. P. Bean. This model assumes that a critical current flows in the sample so as to prevent the penetration of flux into the sample when the magnetic field exceeds H_{c1} and that any changes in the flux distribution are introduced at the sample surface.[10,11]

The measured magnetization of a superconductor is generally a sum of at least two terms:

$$M = M_{eq} + M_{irr}.$$

The first is the equilibrium magnetization M_{eq} that is negative in sign and generated by microscopic supercurrents associated with individual vortices. The second term M_{irr} is due to macroscopic, circulating supercurrents with density J_c, whose existence depends on pinning of vortices to prevent their motion.[12]

If we assume that there is no flux pinning, the magnetization of a superconductor develops as follows. As the field is increased from zero, the magnetization will increase as $-4\pi H$, exhibiting the perfect diamagnetism of a superconductor. Above H_{c1}, the flux will penetrate uniformly into the sample as vortices and the negative magnetization will significantly decrease in magnitude. It will continue to decrease as the field is increased

until H_{c2} is reached, at which point the magnetization will be zero, the field distribution in the superconductor will be microscopically uniform, and the sample will be in the normal state. If the field is then decreased, the magnetization curve will reproduce itself in reverse and there will be no hysteresis.[10] The flux moves unimpeded, in and out of the superconductor, without any barrier. In this case, we obtained from the experiment just the thermodynamic, equilibrium magnetization M_{eq}.

If there are significant pinning sites, then the magnetization curve can look entirely different. The magnetization that is obtained experimentally is $M_{eq} + M_{irr}$ in this case. Above H_{c1}, instead of flux moving in freely, the flow of shielding currents up to the critical current will prevent the equilibrium number of vortices from entering the superconductor. The critical state model assumes that a critical current, due to the distribution of pinned vortices, flows uniformly throughout the superconductor (critical state) to shield the applied field. This implies that the field profile is a linearly decreasing function of distance from the edge to the inside of the sample; dB/dx is a constant proportional to J_c. With increasing field, flux penetrates into the entire sample. As the field is further increased and J_c decreases, the field profile changes its slope (Figure 3-5). Finally, as the field approaches H_{c2}, the critical current falls to zero. When the field is then decreased, the critical current now flows in the opposite direction to prevent the flux from leaving the sample. The magnetization becomes positive because the internal field is actually larger than the applied field, due to the excess flux trapped inside. There is considerable hysteresis in the magnetization curve, and the hysteresis continues all the way to zero field since there is actually trapped flux even when the applied field is zero.[10]

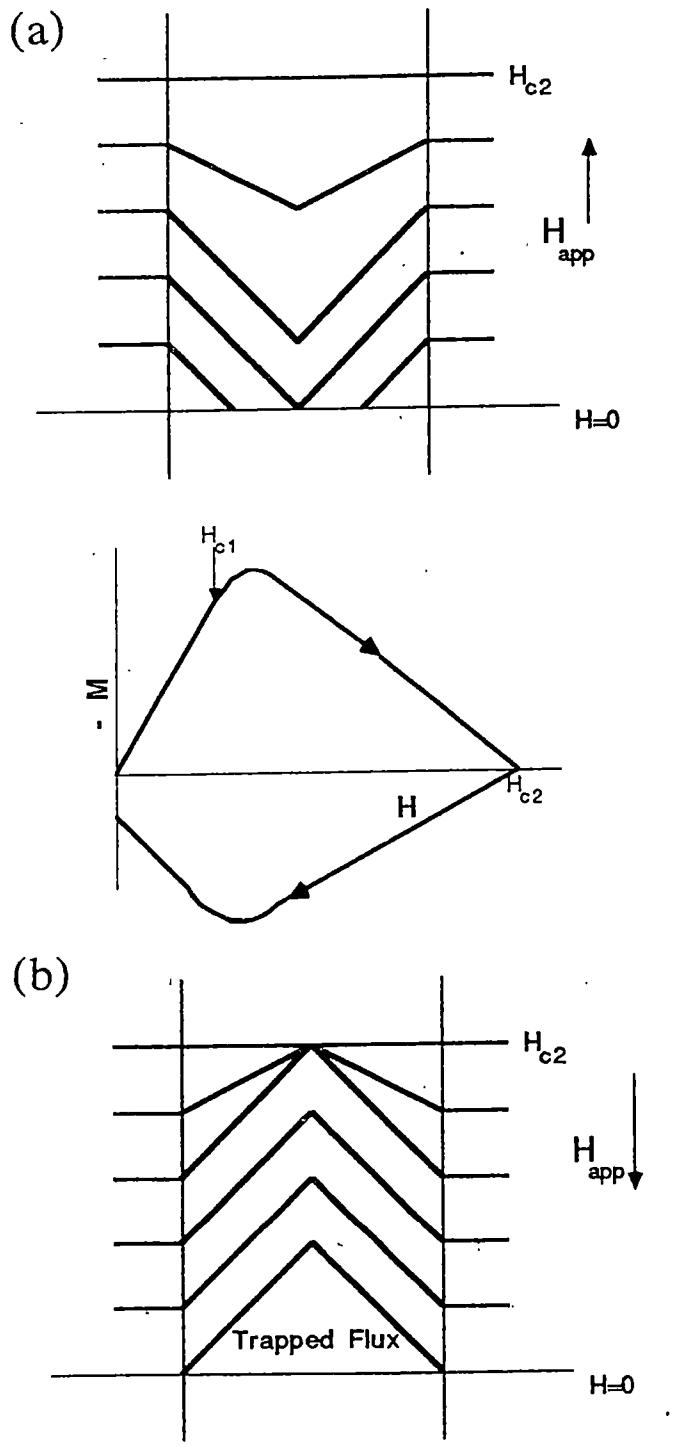

Figure 3-5. The magnetic field profile inside a superconductor and the magnetization curve with pinning. (a) in increasing field and (b) in decreasing field. V. Z. Kresin and S. A. Wolf, "*Fundamentals of Superconductivity*," Plenum Press, New York (1990).

The critical state model provides that the critical current at any field value is directly proportional to $\Delta M = M^- - M^+$, where M^+ and M^- are the magnetization values in increasing and decreasing field history, respectively, in units of emu/cm^3. For the case of a cylinder of radius R (in cm) with field applied parallel to its axis, the critical current density, J_c, is given by

$$J_c = \frac{15 \cdot (M^- - M^+)}{R}$$

in A/cm^2. For a rectangular solid with field perpendicular to a face with sides $L_2 > L_1$, the "sandpile" model provides that

$$J_c = \frac{20 \cdot (M^- - M^+)}{L_1 \cdot (1 - L_1/3 \cdot L_2)}.$$

3.5 The Josephson Junction

If a voltage difference is applied between the two conductive materials that are separated by a thin insulating layer, the wave property of an electron can cause a tunneling current to flow across the insulating layer. However, in 1962, Josephson predicted that a supercurrent could flow between two superconducting electrodes separated by a thin insulating barrier without any voltage difference. A zero voltage tunneling supercurrent flows according to the equation,

$$I = I_c \sin(\phi_1 - \phi_2)$$

where ϕ_1 and ϕ_2 are phases of each superconductors at the tunneling junction and I_c, the critical current, is the maximum supercurrent which can flow across the Josephson junction (the dc Josephson effect).

The phase of a superconductor, or of a Cooper pair-wave, can be changed by a magnetic field which is parallel to the cross section plane of the Josephson junction; which is perpendicular to the tunneling current flow. Therefore, the tunneling current can be changed by the magnetic flux Φ in the plane of the junction, according to the equation,

$$I = I_c \frac{\sin(\pi\Phi/\Phi_0)}{\pi\Phi/\Phi_0}$$

where $\Phi_0 = hc/2e = 2.07\times10^{-7}$ G-cm^2 is the magnetic flux quantum.

It has been observed that the tunneling current drastically decreases and periodically becomes zero when the magnetic flux Φ in the plane of a junction is a multiple of the flux quantum, Φ_0 (Figure 3-6). The magnetic flux-dependent pattern of a tunneling current is analogous with a Fraunhofer diffraction pattern of light.

Josephson also derived that if the voltage difference V were maintained across the junction, the phase difference would change in time and an alternating current would flow according to

$$I = I_c \sin(\phi_0 + \frac{2eV}{\hbar}t)$$

where ϕ_0 is the phase difference at $t = 0$ (the ac Josephson effect).

Although Josephson predicts the effects based on an insulating barrier layer between two superconductors, the effects are more general. Those effects occur

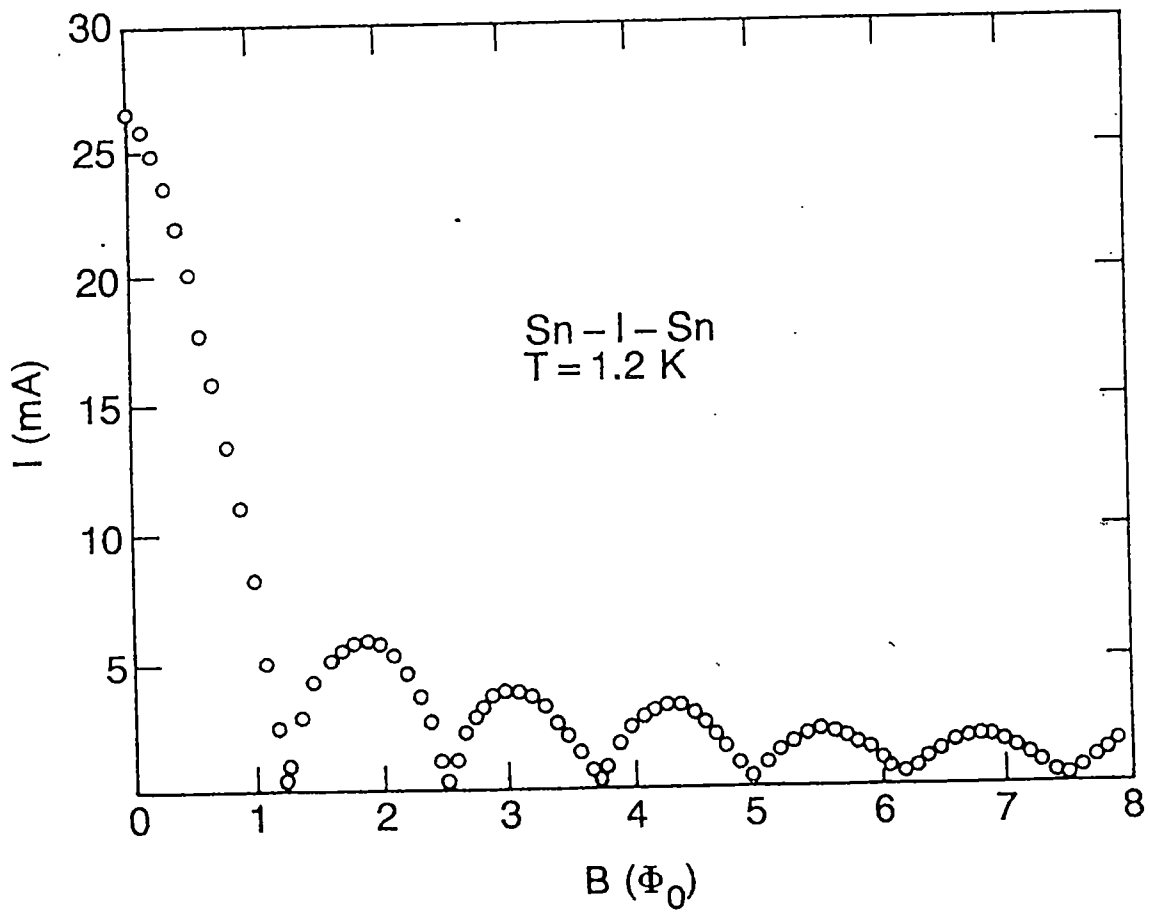

Figure 3-6. Josephson current as a function of magnetic field.
V. Z. Kresin and S. A. Wolf, "*Fundamentals of Superconductivity*," Plenum Press, New York (1990).

whenever two superconductors are connected by a "weak link." The weak link can be an insulating layer between two superconductors (a *S-I-S* junction), or a normal metal layer made weakly superconductive by the *proximity effect,* in which Cooper pairs diffuse into the normal metal (a *S-N-S* junction), or a short, narrow constriction in continuous superconducting material (a *S-c-S* junction).[13] The critical current I_c is, then, a measure of how strongly the phases of the two superconducting electrodes are connected through the weak link. This depends on how thin and of what material the barrier is, or, for constriction weak links, on the cross-sectional area and length of the neck.[13]

In the high temperature superconductors, a grain boundary can serve as a weak link because these materials have such short coherence lengths. Depending on the details, it may be closer to *S-N-S* or *S-I-S* in character.

3.6 Grain Boundaries

Defects can determine the electrical transport properties of solids. Usually, the resistance in a material occurs due to the imperfection in the sample lattice, such as defects, vacancies, etc. While not significantly affecting the critical current densities of conventional superconductors, grain boundaries, an extended defect, in a high-temperature superconductor disappointingly reduce the critical current density by forming weak links.[14] The critical current density J_c decreases exponentially with increasing grain boundary misorientation angle. A transition from low angle to large

angle grain boundaries has frequently been offered as an explanation for the onset of the Josephson behavior at misorientation angles of $\cong 10^{\circ}$.[15]

Several possible mechanisms to explain the origin of the weak-link behavior of large angle grain boundaries in high temperature superconductors have been suggested; they are based on the structural properties of the grain boundaries, deviations from the ideal stoichiometry, and the order parameter symmetry.[15]

First of all, grain boundaries are structural defects that interrupt the lattice structure of the adjacent crystal. Transmission electron microscopy (TEM) studies have shown that the structure of grain boundaries in high-temperature superconductors can be described by standard dislocation theory.[16~18] Consequentially, an array of separate dislocations is formed at a grain boundary. As the misorientation angle increases further, dislocation cores become closer and the effective structural width of a grain boundary increases. With the stain associated with the grain boundary dislocations, various effects arise; the pairing interactions of the superconductor are depressed, the electronic structure of the superconductor is modified, and quasiparticle scattering is enhanced. These effects lower the superconducting order parameter at the grain boundary interface.[15] Extending these ideas, J. Mannhart suggested that the altered electronic structure of the grain boundary leads to a bending of the electronic band structure of the superconductor, which causes depletion layers next to the interface.[15,19] In these layers, the order parameter will be reduced, and for strong enough depletion, the cuprates will be driven into their antiferromagnetic, insulating state.[15,20]

The second view is that deviations from the ideal composition and an impurity segregation at grain boundaries are responsible for their weak-link behavior. However,

this view was ruled out by a scanning transmission electron microscope studies in the Z-contrast mode.[21] The studies show that chemical segregation does not necessarily occur at grain boundaries. Moreover, grain boundary junctions without impurity phases and the correct chemical stoichiometry also show weak-link behavior. However, the STEM analysis is quite insensitive to oxygen because of its relatively low atomic number. The presence of defects in the oxygen sub-lattice will depress the superconducting order parameter, and if the oxygen concentration is low enough, it will drive the grain boundary insulating.

Third, microscopy studies have revealed that grain boundaries are comprised of facets having various orientations. Together with the $d_{x^2-y^2}$ symmetry of the order parameter of high T_c-cuprates, facets on a grain boundary reduce the critical current density J_c with increasing grain boundary angle.[22] However, the study shows that the effect of the faceting together with $d_{x^2-y^2}$ symmetry can account for only a minor part of the experimentally observed reduction of J_c; it causes a depression of critical current density by one to two orders of magnitude for thin films, as the misorientation angle is increased from 0 to 45°.[15]

A recent study, based on the bending of the electronic band structure of the superconductor on a large angle grain boundary, shows that doping of calcium in $YBa_2Cu_3O_{7-\delta}$ increases the J_c, but only at temperatures much lower than 77 K. A more effective way to enhance the Ca concentration at the $YBa_2Cu_3O_{7-\delta}$ grain boundaries is to make superlattice of $YBa_2Cu_3O_{7-\delta}/Y_{1-x}Ca_xBa_2Cu_3O_{7-\delta}$, so that Ca might diffuse into and along the boundary. This sample exhibited an effective increase of J_c at 77 K.[23]

CHAPTER 4

EXPERIMENTAL RESULT AND DISCUSSION

4.1 Analytical Methods

It was mentioned before that currents or current densities can be determined by measuring their associated magnetic moments, which are related by the equation,

$$\vec{m} = \frac{1}{2 \cdot c} \int (\vec{r} \times \vec{J}(\vec{r})) \cdot d\tau . \tag{4-1}$$

According to Bean's critical state model, it can be assumed that current density of the sample in the vortex state is constant spatially inside the sample. With this assumption, the integration of equation (4-1) depends only on the configuration of current flow. If we solve for a current loop with radius r (Figure 4-1-a), as an example, using polar coordinates, the magnetic moment simply becomes

$$\vec{m} = \frac{1}{2 \cdot c} \int_{\theta=0}^{2 \cdot \pi} \vec{R} \times (\vec{I} \cdot R \cdot d\theta)$$

$$m = \frac{1}{2 \cdot c} \int_{\theta=0}^{2 \cdot \pi} R^2 \cdot I \cdot d\theta$$

$$= \frac{2 \cdot \pi \cdot R^2 \cdot I}{2 \cdot c}$$

$$= \frac{\pi \cdot R^2 \cdot I}{c} \tag{4-2}$$

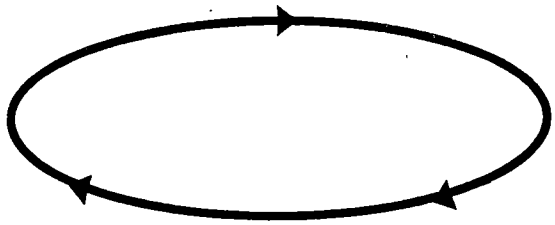

(a) a current loop

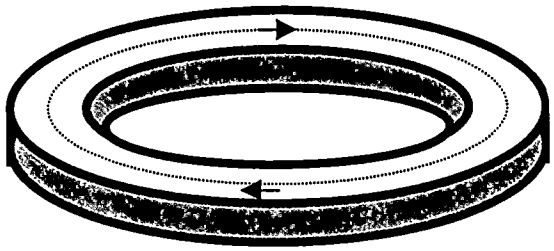

(b) a ring sample

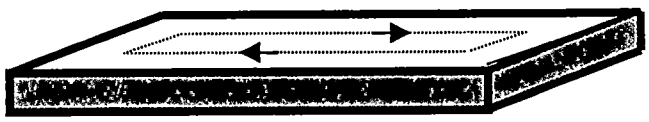

(c) a rectangular sample

Figure 4-1. Current flow in samples with various geometries.

where $\vec{r} = \vec{R}$ is the radius of the circle, and $\vec{J}(\vec{r}) \cdot d\tau = \vec{I} \cdot R \cdot d\theta$ is an element of current. For a ring sample like those used for the experiments (Figure 4-1-b), we can solve the same equation in cylindrical coordinates and obtain

$$m = \frac{1}{2 \cdot c} \int_{r=R_{in}}^{R_{out}} \int_{\theta=0}^{2\pi} \int_{z=0}^{t} r \cdot J \cdot dr \cdot r \cdot d\theta \cdot dz$$

$$= \frac{J}{2 \cdot c} \int_{r=R_{in}}^{R_{out}} r^2 \cdot dr \int_{\theta=0}^{2 \cdot \pi} d\theta \int_{z=0}^{t} dz$$

$$= \frac{2 \cdot \pi \cdot t \cdot J}{2 \cdot c} \cdot \left(\frac{{R_{out}}^3}{3} - \frac{{R_{in}}^3}{3} \right) \qquad (4\text{-}3)$$

where R_{in} and R_{out}, are the inside and outside radius of the ring, respectively, and t is the thickness of YBCO film. Therefore the current density of a sample becomes

$$J_c = \frac{30 \cdot m}{\pi \cdot ({R_{out}}^3 - {R_{in}}^3) \cdot t}$$

$$= \frac{30 \cdot m}{V_{out} \cdot R_{out} - V_{in} \cdot R_{in}} \qquad (4\text{-}4)$$

where V_{out} is the volume of a cylinder with the outer radius R_{out} of the ring, and V_{in} is the volume of the "missing" cylinder with the inner radius R_{in}. This result was used to obtain the current densities of grain rings. By a similar calculation, the current density of a rectangular sample with sides $L_2 > L_1$ (Figure 4-1-c) can be obtained by the "sandpile" model,

$$J_c = \frac{40 \cdot M}{L_1 \cdot (1 - L_1/3 \cdot L_2)} \qquad (4\text{-}5)$$

where $M = m/V$ is the magnetization of the sample. Since the current flow in an open ring sample is analogous to that in a rectangular sample, the equation (4-5) for a rectangular sample can be applied to obtain the current density of an open ring sample, with a small modification. Therefore, for an open ring case, simply replacing $L_1 = R_{out} - R_{in} = w$, $L_2 = 2 \cdot \pi \cdot R$, and using $L_2 >> L_1$, one has from equation (4-5) that,

$$J_c = \frac{40 \cdot m/V}{L_1}$$

$$= \frac{40 \cdot m}{(2 \cdot \pi \cdot R \cdot w \cdot t) \cdot w}$$

$$= \frac{40 \cdot m}{2 \cdot \pi \cdot R \cdot w^2 \cdot t} \qquad (4\text{-}6)$$

More effort is needed to obtain the current density of a GB ring. Since the integral of the equation (4-1) is related to the configuration of current flow, the nature of the current flow in a GB ring should be deduced first. Simply speaking, a grain boundary region can be seen as an area where the current–carrying cross section decreases compared to the grain region, due to an array of insulating dislocation cores and the suppressed superconducting order parameter in the vicinal area of dislocation cores.[24] In the beginning, in the Meissner state and in the vortex state with low applied fields, the entire current induced by a given field in a GB ring can flow across the grain boundary. Therefore, in this case, the feature of current flow in a GB ring is analogous to that of a grain ring. If the current flowing in a GB ring exceeds the maximum current that the grain boundary cross section can support, only a portion of the current flows across the grain boundary (Figure 4-2-a) and the remainder reflects at the grain boundary (Figure 4-2-b). Therefore, there exist two components of current flow in a GB ring in a high field:

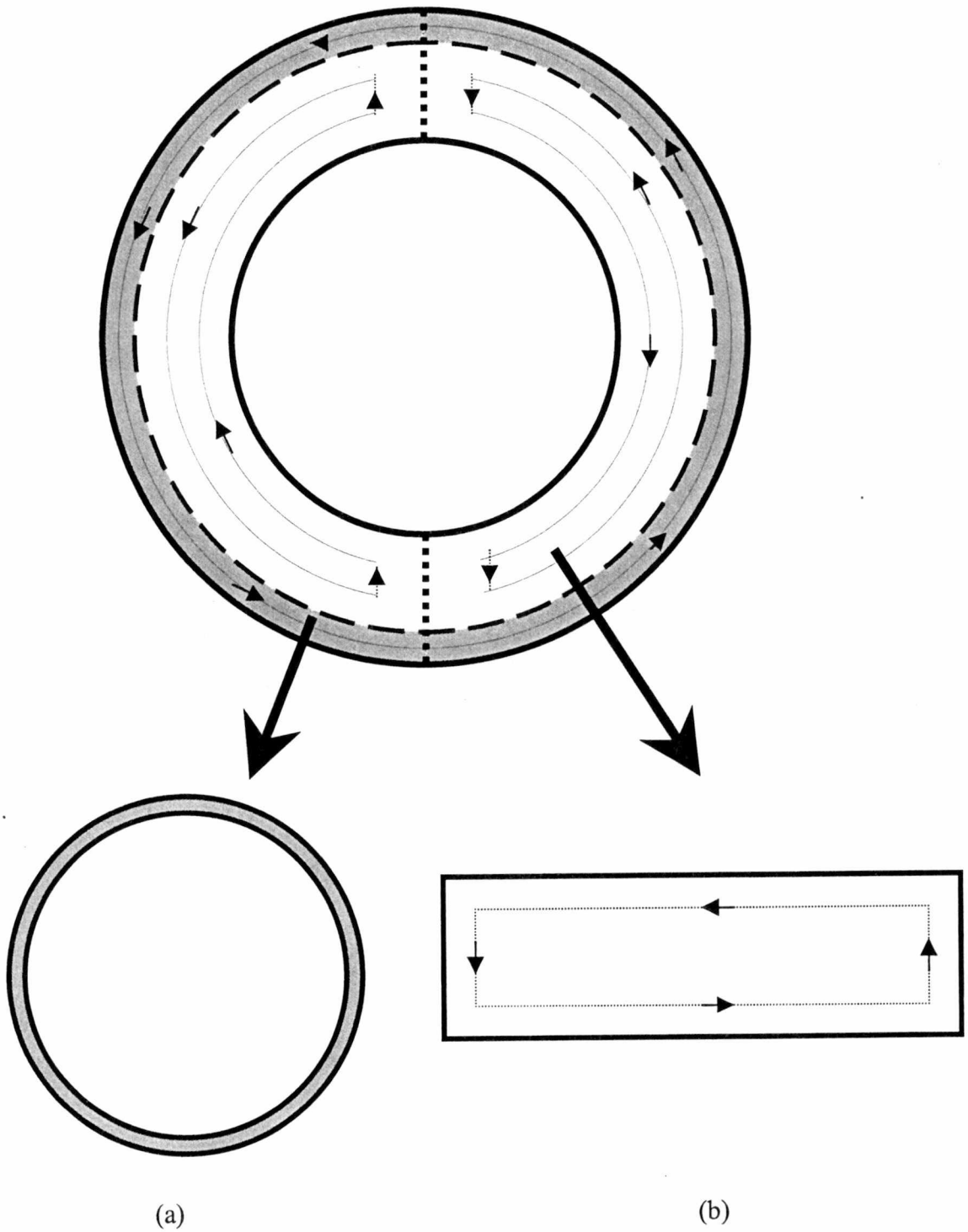

Figure 4-2. Current configurations: (a) ring-like current flow and (b) strip-like current flow.

one is analogous to that in a ring sample and the other is like that in an open ring (strip-like). Those two current distributions contribute a ring-like moment and a strip-like moment, respectively, to the total magnetic moment of the GB ring. In other words, if we can separate the total magnetic moment of a GB ring into ring-like and strip-like moments, then a pure grain boundary current density can be obtained. The equation (4-1) becomes

$$\vec{m}_{GB} = \vec{m}_{ring} + \vec{m}_{strip}$$

$$= \frac{1}{2 \cdot c} \int_{ring} (\vec{r} \times \vec{J}(\vec{r})) \cdot d\tau + \frac{1}{2 \cdot c} \int_{strip} (\vec{r} \times \vec{J}(\vec{r})) \cdot d\tau. \qquad (4\text{-}7)$$

Let us assume that a real GB current which is a ring-like, I_{GB} flows within a width d, and that a strip-like current, I_{strip} flows within the remaining width, w-d (Figure 4-3). For the case of $d << w$, a ring like current can be treated like a one-dimensional current loop. The equation (4-7) simply becomes

$$m_{GB} = \frac{1}{10} \cdot J \cdot t \cdot d \cdot \pi \cdot R^2 + \frac{1}{40} \cdot J \cdot t \cdot 2 \cdot \pi \cdot R \cdot (w-d)^2 \qquad (4\text{-}8)$$

where c=10 in lab units (i.e., moments in emu, current density in A/cm^2, and lengths in cm). The important thing is that the current densities for both a ring-like and a strip-like current flows are same but those currents values are different. The intrinsic critical current density of GB and of its companion grain rings at a certain temperature and field should be same because they are originally from one film. Therefore the current density J in equation (4-8) must be replaced by a grain current density J_c^{Gr} and the equation becomes

$$m_{GB} = \frac{1}{10} \cdot J_c^{Gr} \cdot t \cdot d \cdot \pi \cdot R^2 + \frac{1}{40} \cdot J_c^{Gr} \cdot t \cdot 2 \cdot \pi \cdot R \cdot (w-d)^2. \qquad (4\text{-}9)$$

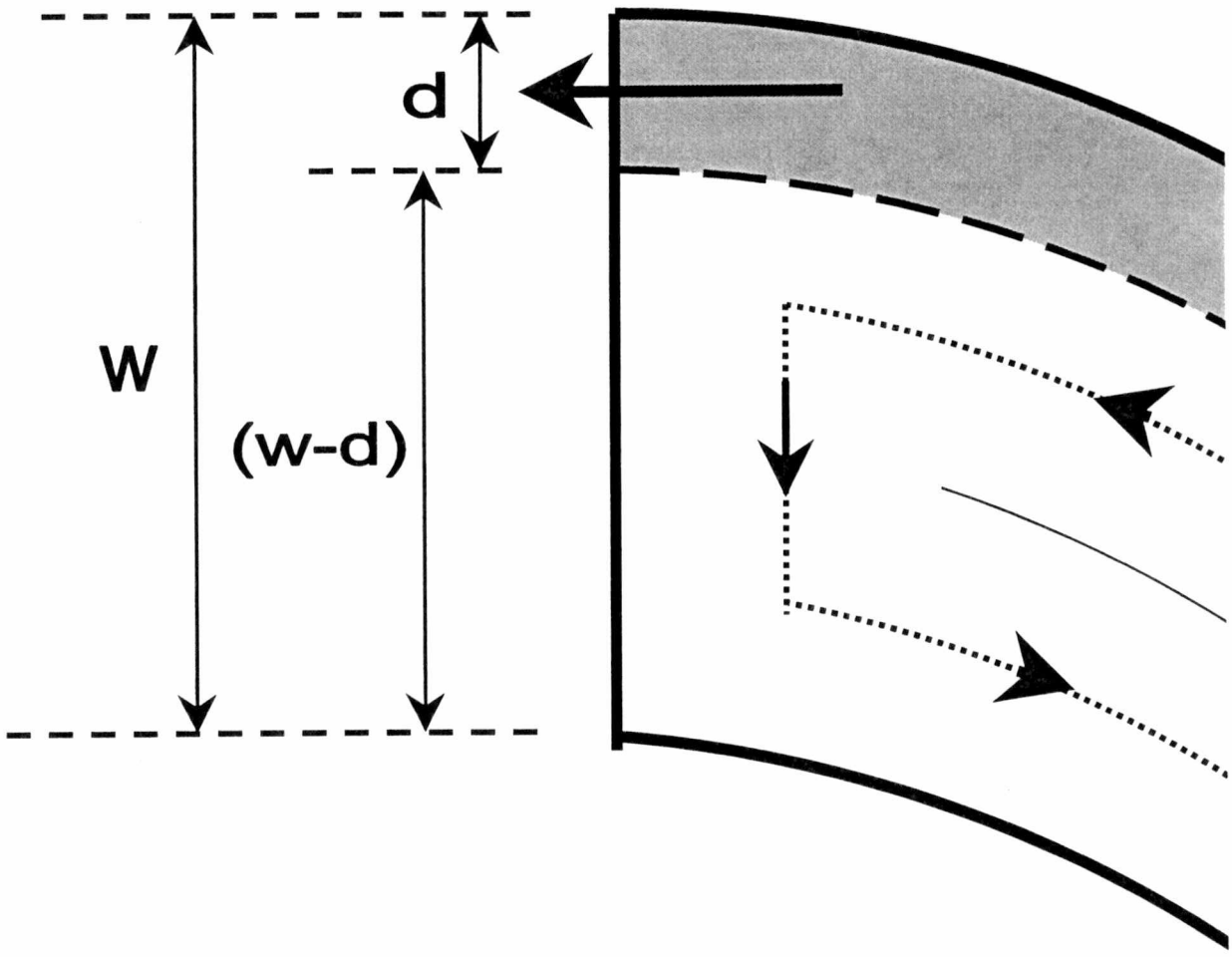

Figure 4-3. Detailed current flow near a grain boundary.

At this point, let us note that there are two unknowns in this equation: the grain current density J_c^{Gr}, which can be measured separately on a grain ring; and the fractional width (d/w), which can be obtained from this expression by measurement of m_{GB}. By further calculation, a simpler and useful form of this equation can be obtained,

$$\frac{d}{w} \cong \frac{m_{GB} - m_{op}}{m_{Gr} - 2 \cdot m_{op}} \tag{4-10}$$

where m_{GB}, m_{Gr}, and m_{op} are magnetic moments of GB, a companion grain, and an open ring, respectively. Therefore, if magnetic moments of a companion grain and an open rings (which differ only by geometrical factors) are given at a certain temperature and field, then the equation (4-10) will give the width of a ring-like current in a GB ring sample under the same circumstances. Finally, a true GB current density, J_c^{GB} can be obtained by using the continuity equation with a width d,

$$J_c^{Gr} \cdot t \cdot d = J_c^{GB} \cdot t \cdot w$$

$$J_c^{GB} = J_c^{Gr} \cdot \left(\frac{d}{w} \right). \tag{4-11}$$

Inserting the equation (4-10) into the equation (4-11) gives

$$J_c^{GB} = J_c^{Gr} \cdot \left(\frac{m_{GB} - m_{op}}{m_{Gr} - 2 \cdot m_{op}} \right). \tag{4-12}$$

However, both m_{Gr} and m_{op} are created by same grain current density, J_c^{Gr}, and their values differ only because of geometrical differences, i.e. different current distributions. Therefore, the pure grain boundary current density J_c^{GB} in equation (4-12) only depends

on the measured magnetic moment of a GB ring and its grain current density J_c^{Gr} which are obtained in two separate experiments.

All the GB current density values that we will discuss in the experimental results and analysis part were obtained using equation (4-12). For a grain and an open rings, equation (4-4) and equation (4-6) were used, respectively.

4.2 Results of Temperature Sweep Experiments

All of the grain, GB, and open rings had the same T_c, near 93 K. Typical grain current density values, J_c^{Gr}, were 34 ~ 39 MA/cm^2 in zero applied field for good samples. Figure 4-4 shows that even though the magnetic moment of an open ring was significantly smaller than that of a grain ring (Figure 4-4-a), because of differences of sample geometry, commensurate values of the critical current density were obtained from both rings in the whole temperature range (Figure 4-4-b).

On the other hand, Figure 4-5 shows that the current densities J_c^{GB} of the GB rings (except for 1.8°) are lower than the values of grain rings, for the entire temperature range. For the 1.8° GB samples (Figure 4-5-a), the current density values at 5 K were 35~36 MA/cm^2, which were not significantly different from the values of grain rings. Moreover, the temperature-dependent current density curves of the 1.8° GB rings are not significantly different from those for the grain rings.

Figure 4-6 shows the temperature-dependent current density curves of 1.8°, 2.8°, 5.1°, and 7° grain boundary samples. The grain boundary current density decreases as the

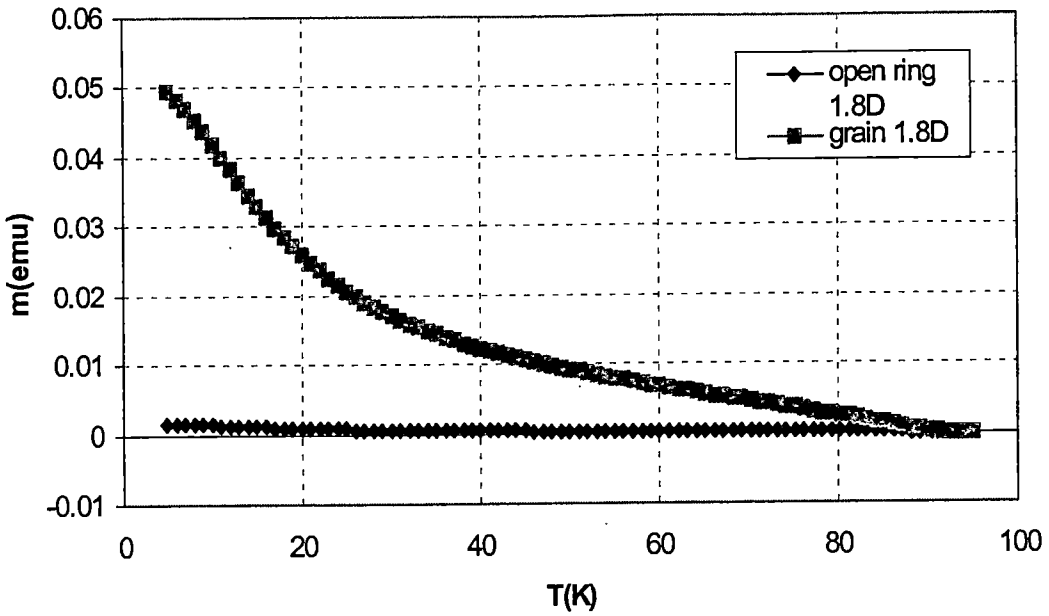

(a)

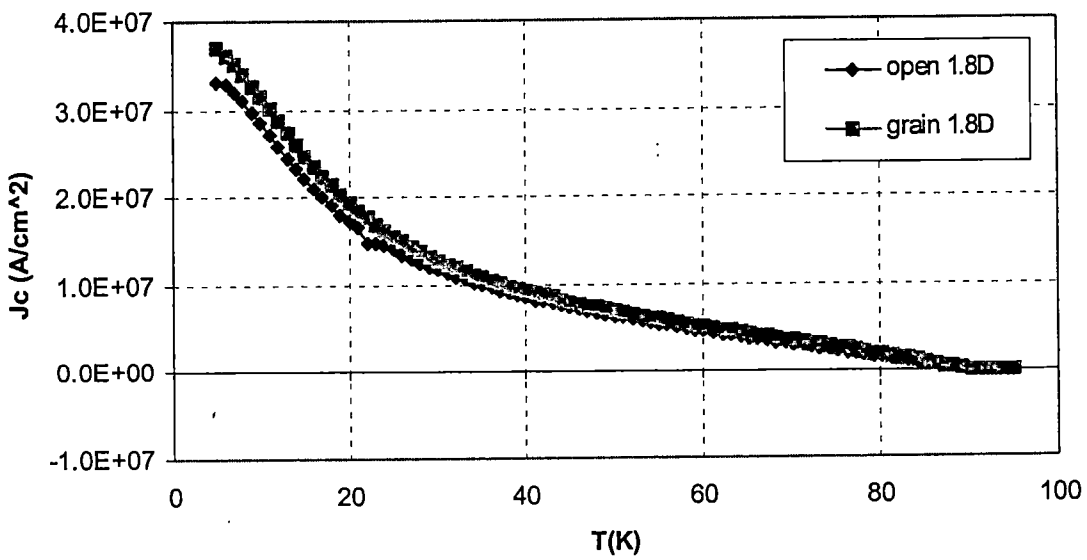

(b)

Figure 4-4. A comparision of 1.8° grain and open rings: (a) magnetic moment versus temperature and (b) current density versus temperature.

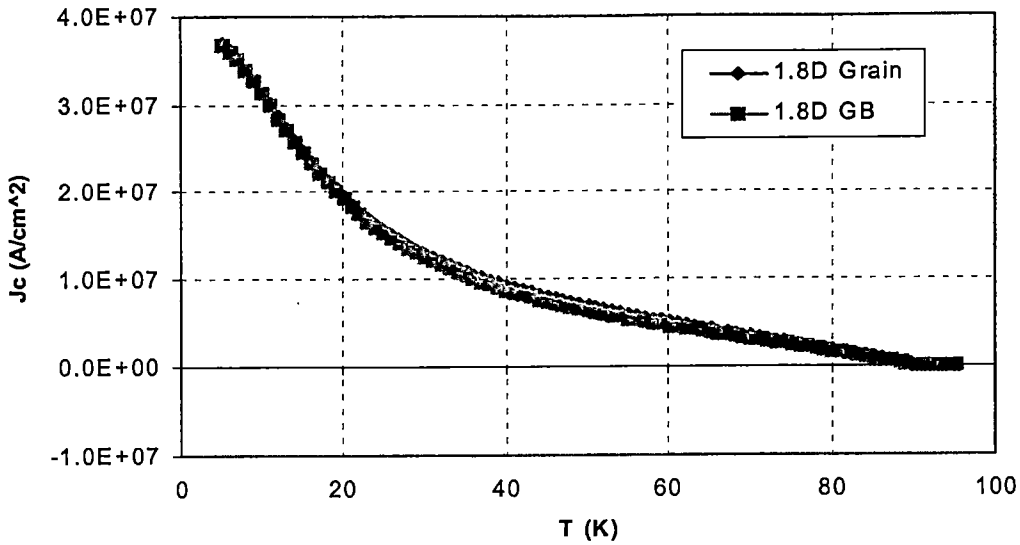

(a)

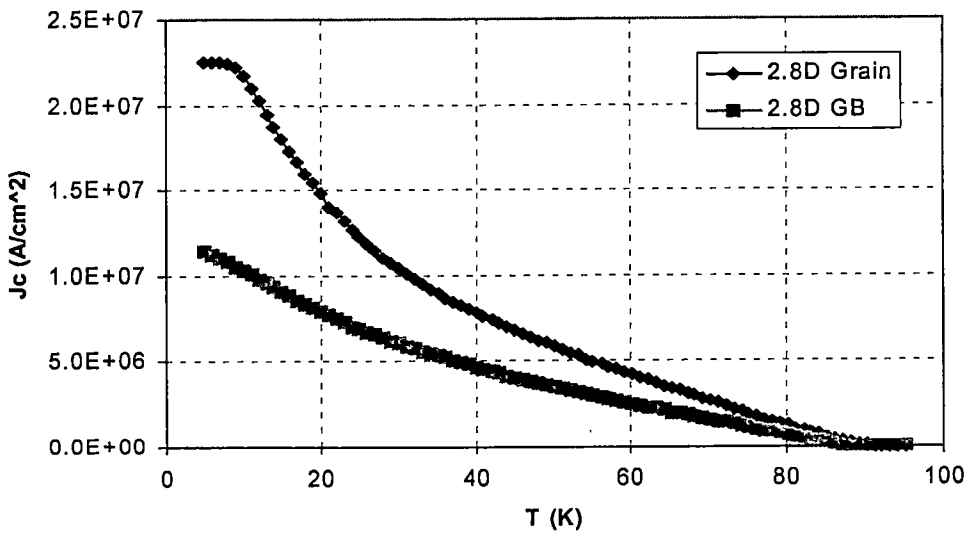

(b)

Figure 4-5. Current density versus temperature at 5 K for a GB and its companion grain ring. (a) 1.8° and (b) 2.8° samples.

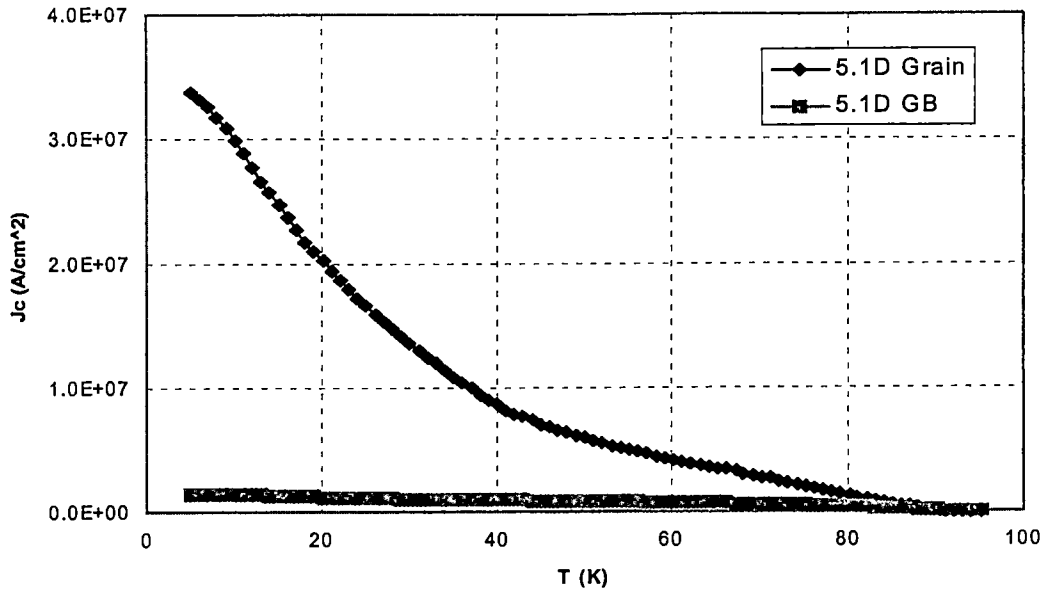

(c)

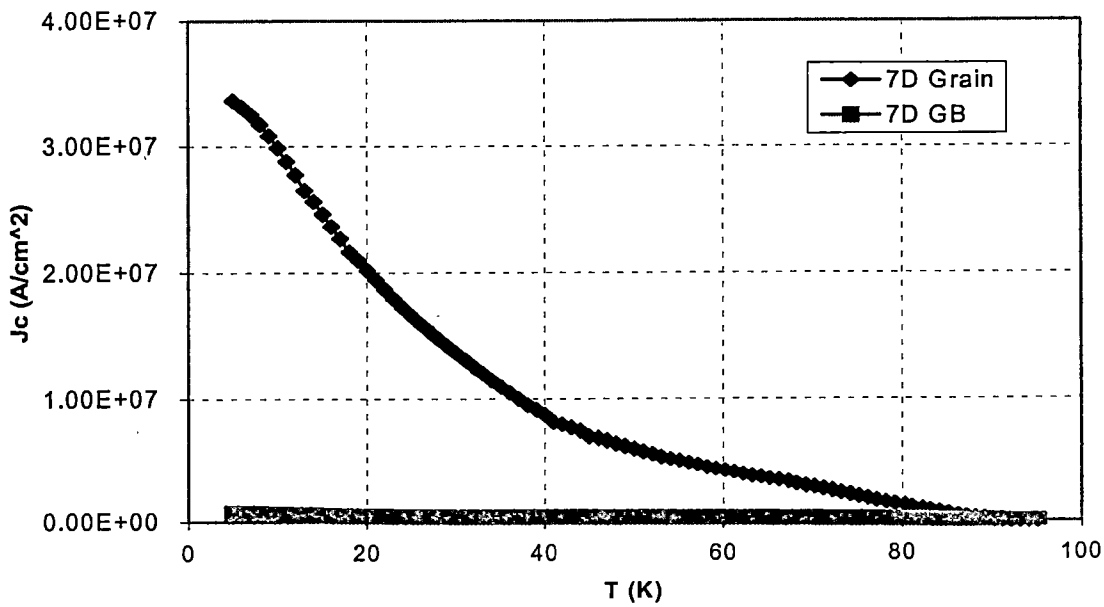

(d)

Figure 4-5 (continued). (c) 5.1° and (d) 7° samples.

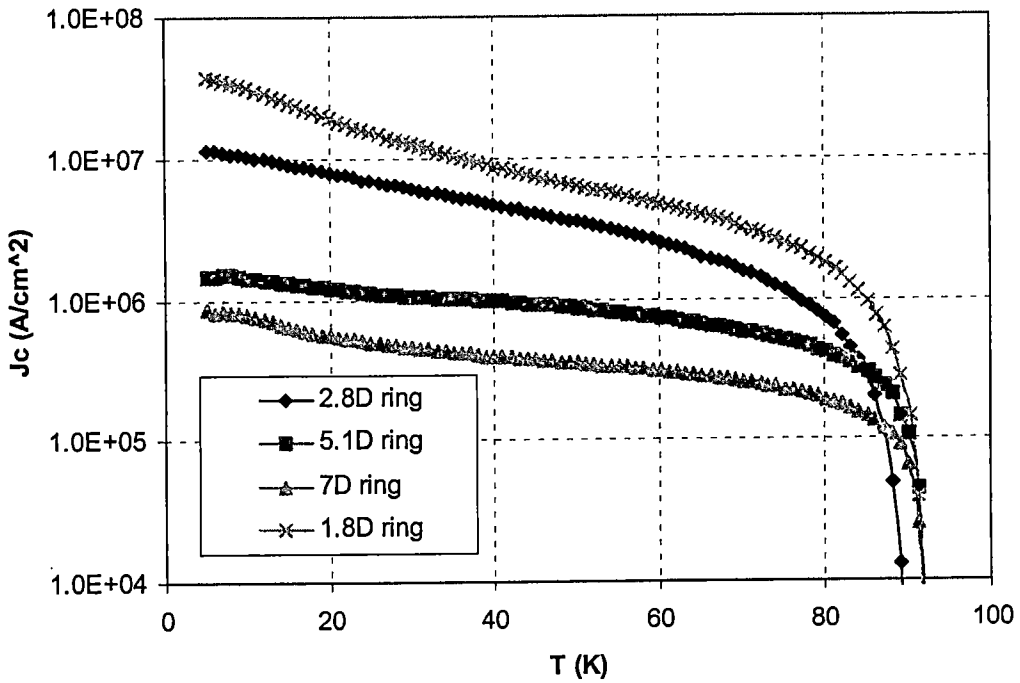

Figure 4-6. Grain boundary current density versus temperature plotted in logarithmic scale.

angle of a grain boundary increases. Even though the 2.8° grain boundary significantly reduces the current density, still its current density values are larger than for the 5.1° and 7° grain boundary samples. Figure 4-7 shows that the GB current densities at a fixed temperature decrease exponentially with increasing misorientation of the grain boundary. A huge diminutions of the grain boundary current density occur between 1.8° and 2.8° and between 2.8° and 5.1°, whereas there is a relatively small diminution between 5.1° and 7°. This suggests that a small angle grain boundary with an angle $1.8^\circ < \theta < 5.1^\circ$ strongly impedes the current flowing across it. More precisely, since no difference between 1.8° GB and grain rings was observed, the range $1.8^\circ \le \theta \le 2.8^\circ$ seems to contain the critical angle where a grain boundary begins to execute its important impact on current flowing across the grain boundary. Therefore, the current density of a sample is likely to be strongly influenced by misorientations in the sample of only a few degree.

Since we have calculated a value of d/w to obtain J_c^{GB}, the partitioned moment coming from just a strip-like current flow can be calculated. Using equation (4-6), the strip-like partitioned moment of a GB ring sample can be obtained by

$$m_{strip} = \frac{2 \cdot \pi \cdot R \cdot t \cdot (w-d)^2 \cdot J_c^{Gr}}{40}. \qquad (4\text{-}13)$$

The resulting strip-like partitioned moments of all GB ring samples were always smaller than the moments of an open ring at all temperatures (Figure 4-8); especially the strip-like partition moment of 1.8° GB ring sample is almost negligible. This supports the idea that there exist two features of current flow in a GB sample (except 1.8°), and the current flowing across a grain boundary I_{GB} subsists up to the critical temperature for all angles,

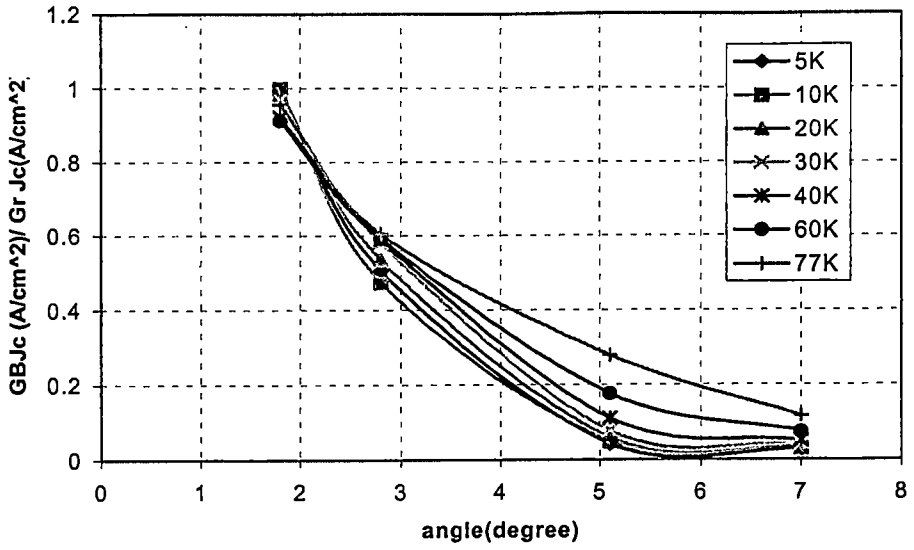

(a)

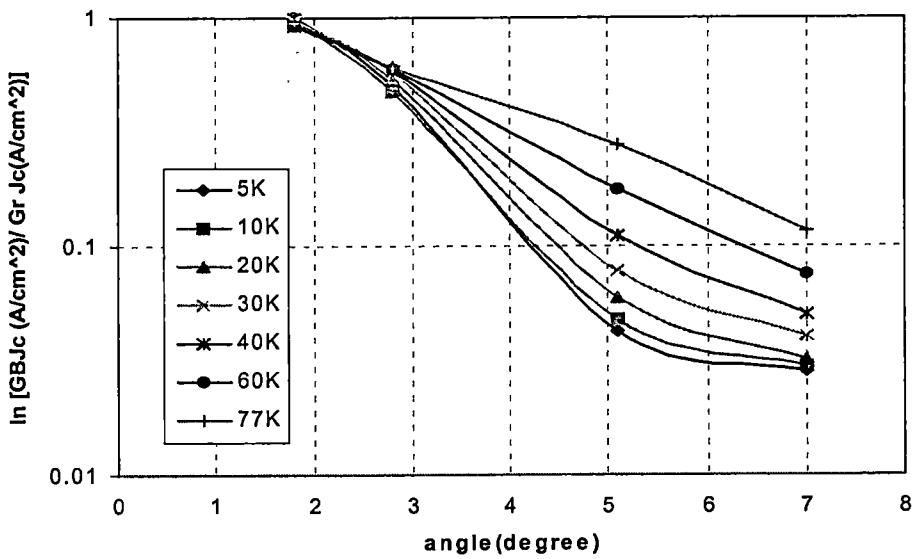

(b)

Figure 4-7. GB current density (normalized) versus misorientation angle. (a) normal scale and (b) logarithmic scale.

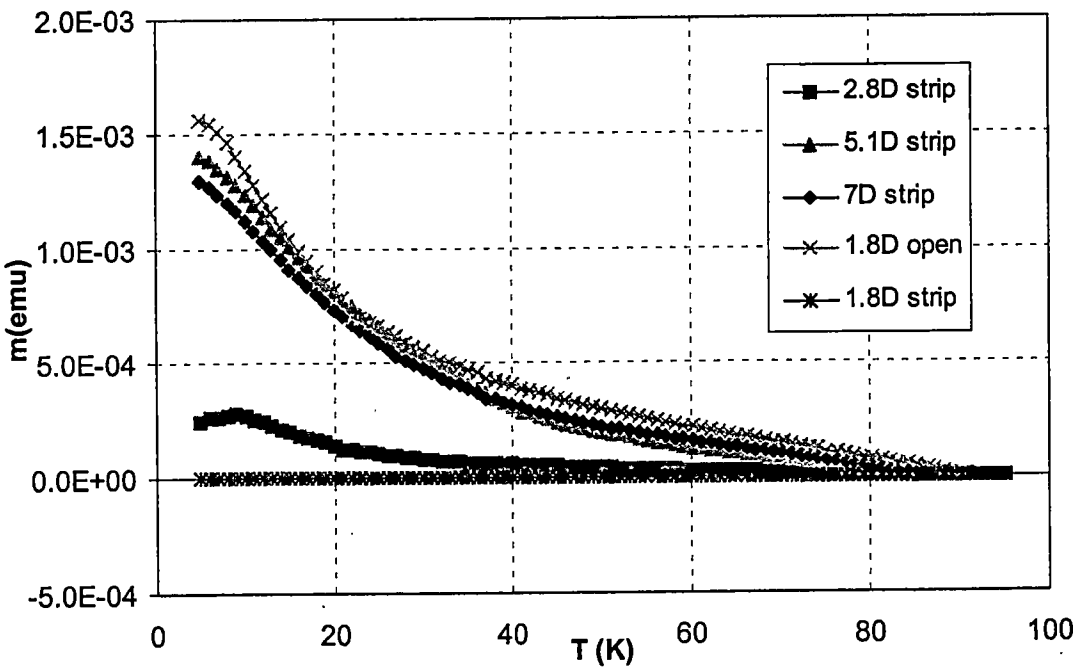

Figure 4-8. Strip-like moment versus temperature.

1.8°, 2.8°, 5.1°, and 7°. As is seen in Figure 4-8, the smaller the grain boundary angle is, the less the strip-like partition moment contributes to the total moment of the grain boundary ring. It follows that the bad insulating cross section areas increased as the the angle of a grain boundary increased.

4.3 Results of Field Sweep Experiments

All the as-obtained data were background-corrected by subtracting the moments of Si mounting disks and other contamination from the raw data. Nicely symmetric curves of magnetic moment versus field were obtained from all the grain and open ring samples (Figure 4-9). As was seen in the temperature sweep experiments, open ring moments were smaller than the grain ring moments in whole field range at all temperatures. In increasing applied fields, maximum negative moments for virgin samples were obtained at the field of full penetration, 100 Oe field for grain rings and 500 Oe field for open rings. This field difference is, as mentioned, due to the different sample geometry. When the applied field decreased back from its maximum of 65 kOe to zero, the maximum positive moments of open and grain rings were obtained. Critical current densities were calculated using equations (4-4) and (4-6) for grain and open rings, respectively. The open ring and grain ring have almost the same critical current density values, as a function of field and temperature (Figure 4-10). A rapid decrease of current density due to increasing field was seen up to 10 kOe. After that, the decrease of current

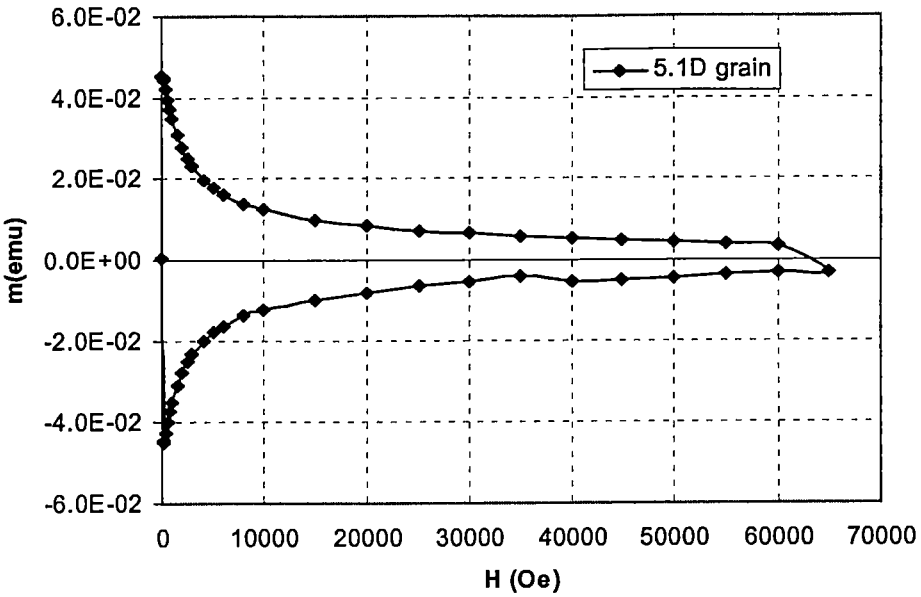

(a)

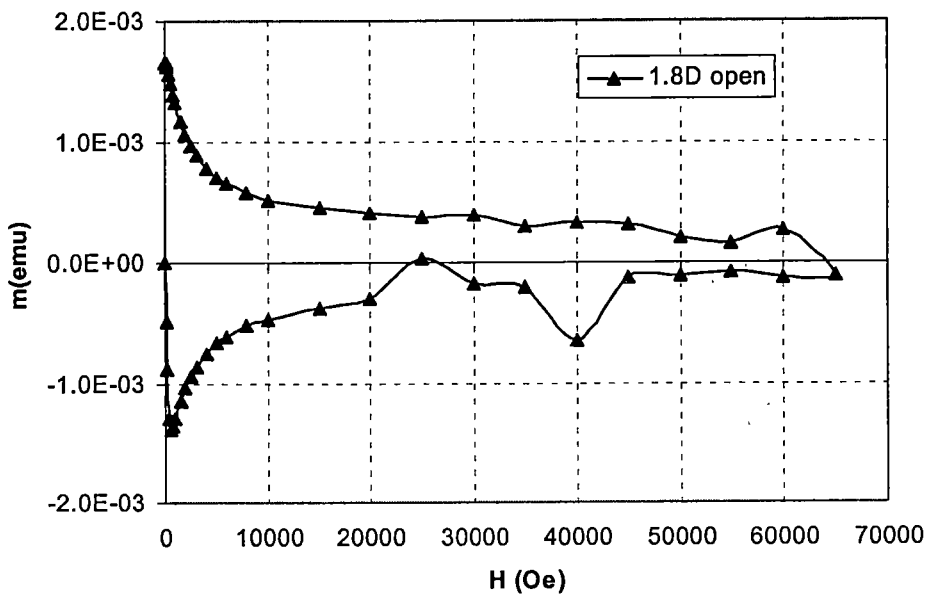

(b)

Figure 4-9. Magnetic moment versus field at 5 K.
(a) 5.1° grain ring and (b) 1.8° open ring.

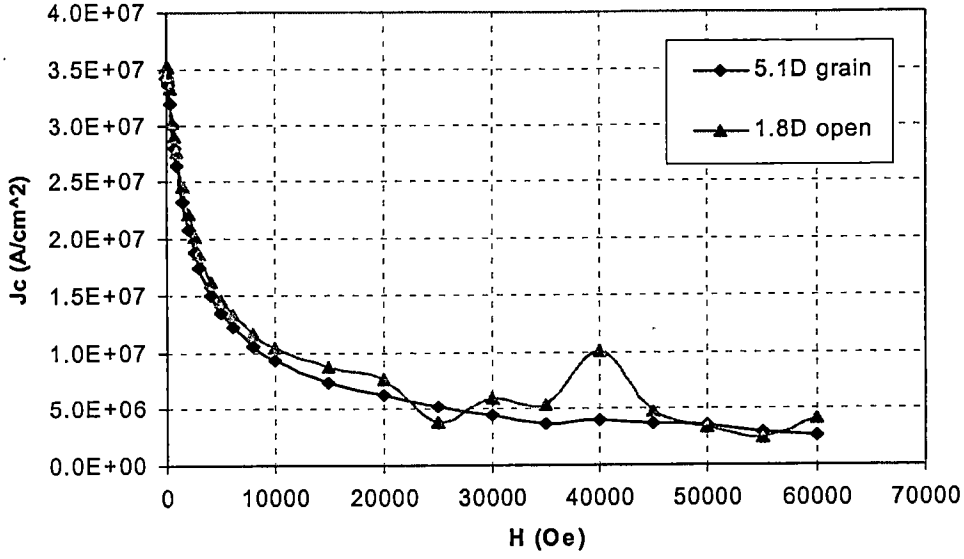

(a)

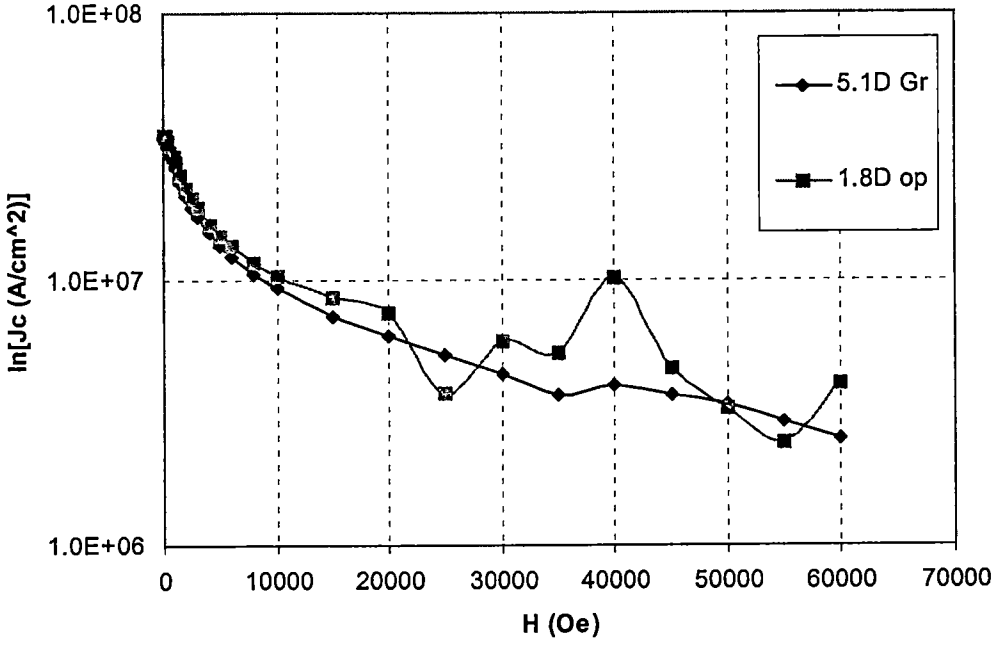

(b)

Figure 4-10. Current density versus field for 5.1° grain and 1.8° open rings at 5 K. (a) normal scale and (b) logarithmic scale.

densities is rather slower. Current density values corresponding to maximum moments at all temperatures matched well with values obtained from temperature sweep experiment. In the temperature sweep experiment, no differences were found between 1.8° GB and companion grain rings in magnetic measurement studies. The curves of m versus H for the 1.8° GB rings were as symmetry as those of grain rings, with very similar values of magnetic moment in the entire field range (Figure 4-11-a). Therefore, the magnetic field dependence of the critical current densities of the 1.8° GB and its companion grain ring are almost the same (Figure 4-11-b).

However, the 5.1° and 7° GB ring samples differ considerably from the grain ring or open ring samples in their $m(H)$ curves (Figure 4-12-a, and b). Magnetic moments of those 5.1° and 7° GB ring samples were smaller than the grain rings but larger than open rings. Furthermore, the appearance of huge peaks in the m versus H curves while decreasing the applied field from 65 kOe was a distinct feature of the 5.1° and 7° GB rings. Notice that in increasing magnetic field, the $m(H)$ curves of the 5.1° and 7° GB rings are similar to those of open rings; in decreasing fields, those curves are similar to grain rings down to the peak fields. In increasing fields, currents flowing across grain boundaries seem to create larger total magnetic moments in the GB ring samples than magnetic moments of open ring samples, even at high fields. In decreasing fields, the amount of current flowing across grain boundaries somehow increases, so that it contributes to the appearance of huge magnetic moments. When decreasing fields returned to fields of full penetration again, the same values of magnetic moments obtained at the field of full penetration were observed. Further decrease of the field did not change the values of magnetic moments. Magnetic moments stayed at same values

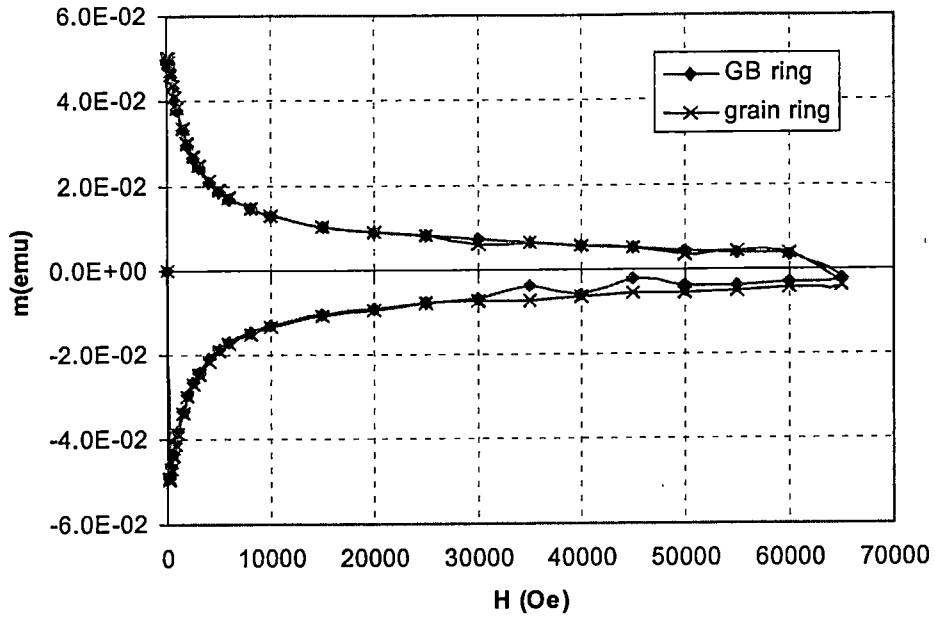

(a)

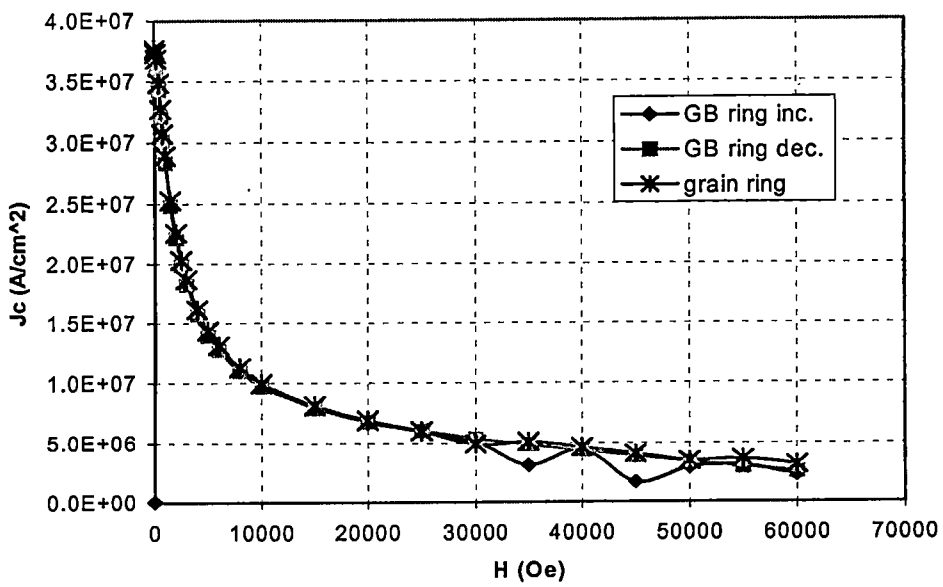

(b)

Figure 4-11. Field dependent magnetic moment and current density of 1.8° GB and companion grain ring samples at 5 K. (a) magnetic moment versus field, and (b) current density versus field.

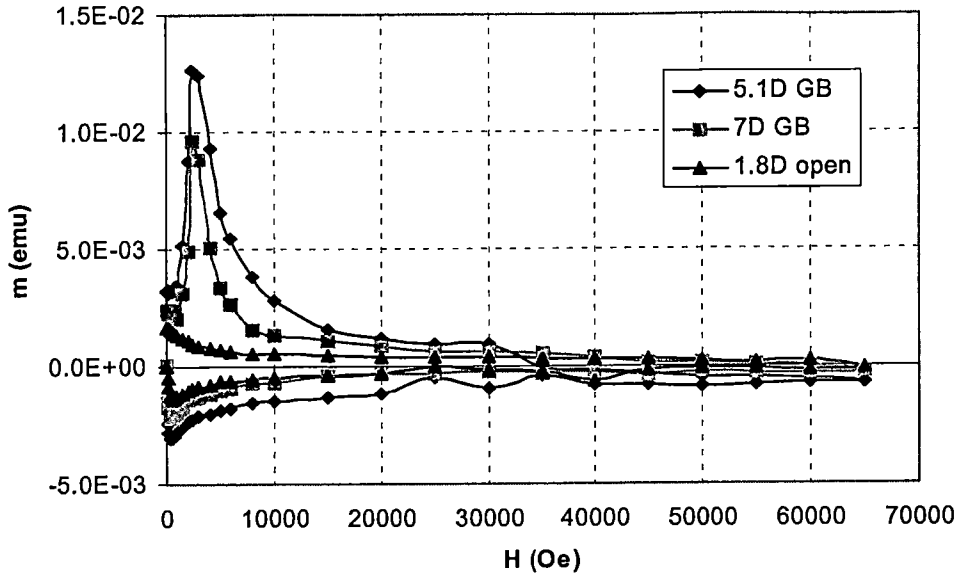

(a)

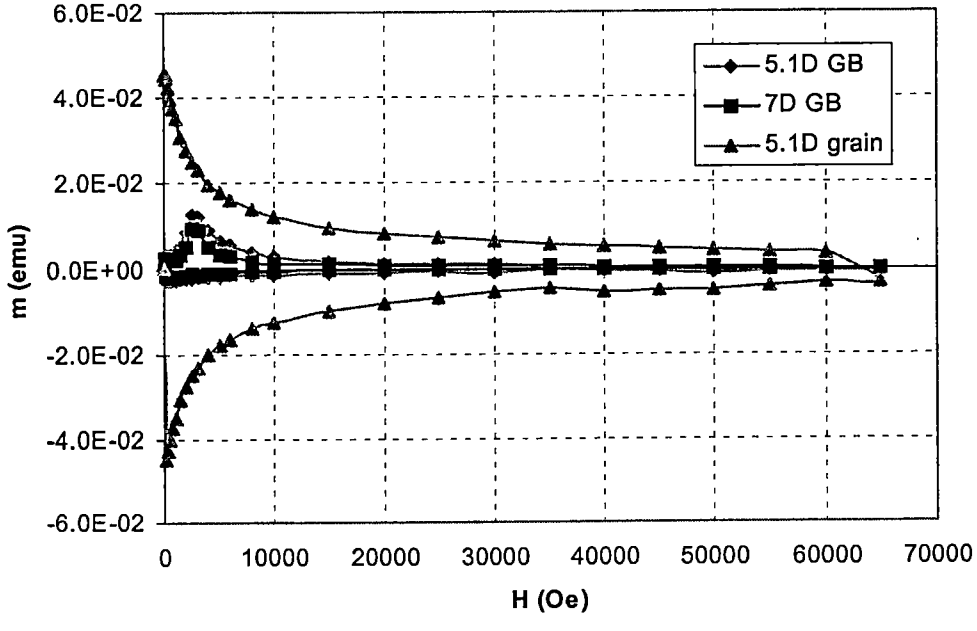

(b)

Figure 4-12. $m(H)$ curves of 5.1° and 7°GB rings comparing with those of grain and open rings at 5 K, (a) with 1.8° open ring and (b) with 5.1° grain ring.

until the applied field was reduced completely to zero. Those moments have similar values with moments measured in temperature sweep experiments. The magnetic moments at peak fields were always much larger than the zero field magnetic moments. As the measurement temperature increased, the peak moment and peak field decreased and the peak feature become more narrow.

For the 2.8° GB ring samples, intermediate behavior was observed in the field sweep measurements as well as in temperature sweep measurements (Figure 4-13). Moments of 2.8° GB ring samples were smaller than those of companion grain samples in the whole field range, like the other GB ring samples. Peaks were also found in decreasing applied field. Those peaks were, however, not as significantly large as those of the 5.1° and 7° GB ring samples and they occurred at very low fields.

The peaks in the $m(H)$ curves of the GB sample occur at applied magnetic fields that decrease with temperature. This variation is shown for the 2.8°, 5.1°, and 7° GB ring samples in Figure 4-14-a. Peaks appeared at similar fields for 5.1° and 7° GB samples, and at lower fields for the 2.8° GB sample. The true values of current density inside the GB samples, which create the peaks in $m(H)$ curves, can be obtained from the current density-data of their companion grain rings (grain current densities were measured at peak fields and given temperatures, also). Current densities of companion grain rings that correspond to peak fields of each GB samples at certain temperatures are shown in Figure 4-14-b. Interestingly, the values of the corresponding grain current densities for each GB samples at given temperatures are similar and they do not seem to depend on the grain boundary angles. Not only are those corresponding grain current density values similar, but also their temperature dependencies are very similar.

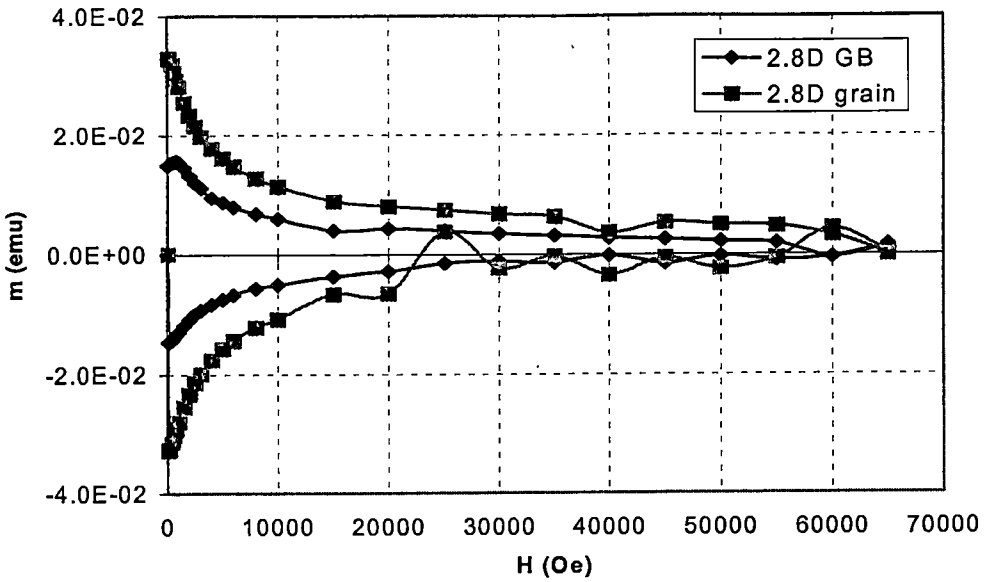

(a)

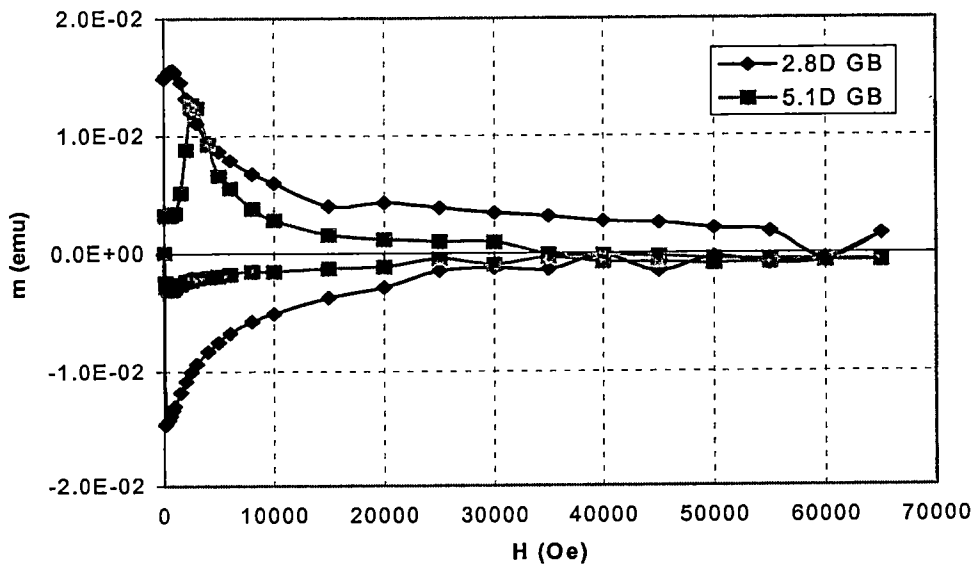

(b)

Figure 4-13. $m(H)$ curves of a 2.8° GB ring, compared with those of companion grain and 5.1° GB rings at 5 K.
(a) with companion grain ring and (b) with 5.1° GB ring.

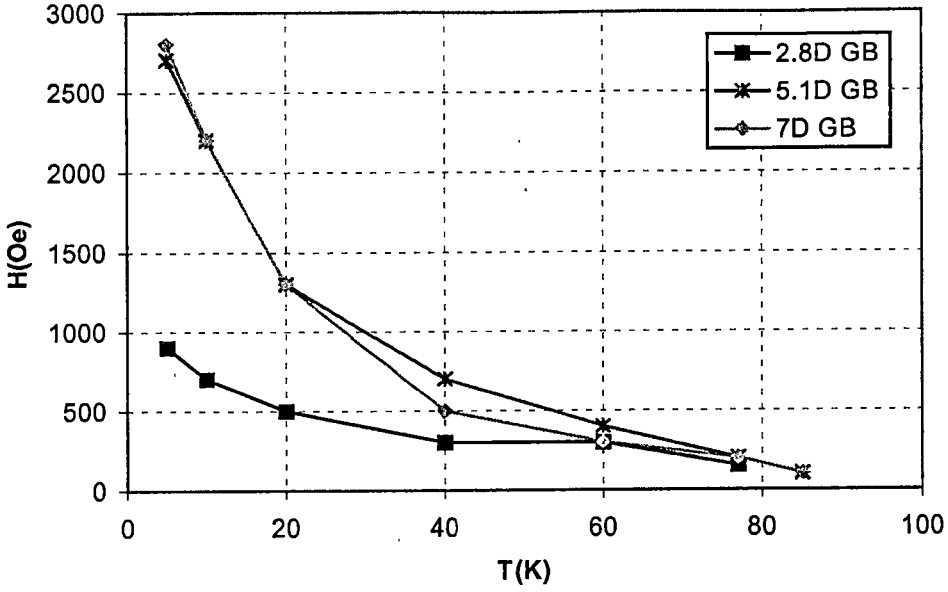

(a)

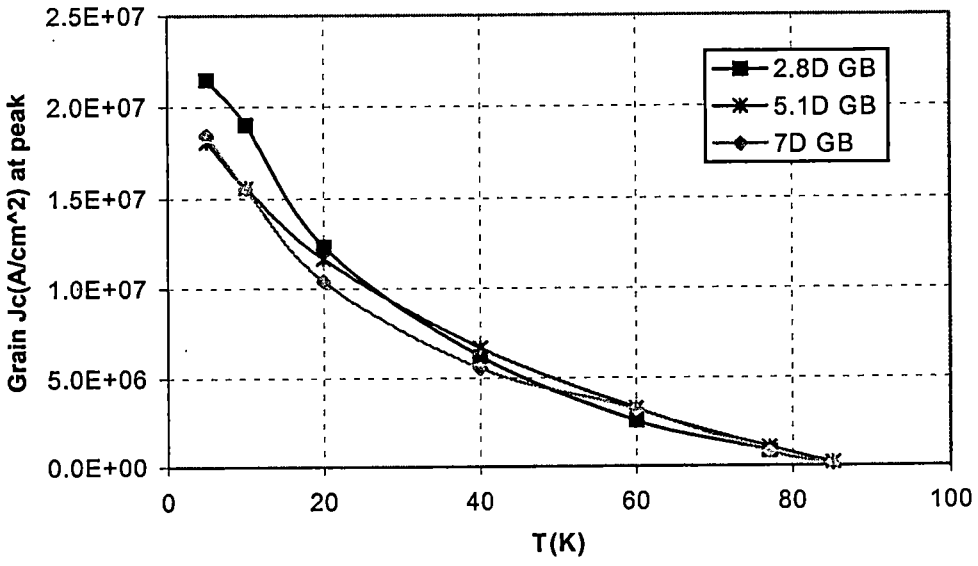

(b)

Figure 4-14. H_{peak} and $J_c^{Gr}(H_{peak})$ versus temperature for 2.8°, 5.1°, and 7° GB rings. (a) H_{peak} and (b) $J_c^{Gr}(H_{peak})$.

The occurrence of a peak in the $m(H)$ curve of a GB sample seems to mark the appearance of weak-link behavior in the small angle grain boundary. It is likely explained by the effect of a magnetic field on a Josephson junction which a grain boundary resembles. It is well known that the maximum tunneling current can flow across a Josephson junction if the net field, which is perpendicular to the tunneling current flow, become zero on the area of the junction. Applying this idea, one might think that the total magnetic field on a grain boundary (H_{local}) becomes roughly zero at the peak field:

$$H_{local} = \sum H \approx 0 . \tag{4-14}$$

The applied magnetic field H_{app} and the field created by the current flowing in the vicinity of the grain boundary H_{self} are the two major fields on the grain boundary. Therefore, H_{local} becomes

$$H_{local} \approx H_{app} + H_{self} \approx 0 . \tag{4-15}$$

Since equation (4-15) should be satisfied at the peak fields, then H_{app} is equal to H_{peak}. Then equation (4-15) becomes

$$H_{peak} \approx H_{self} . \tag{4-16}$$

Since H_{self} is due to the current nearby the grain boundary, the equation (4-16) becomes

$$H_{peak} \propto I_{GB} \propto J_c^{Gr}$$

$$H_{peak} \propto J_c^{Gr} . \tag{4-17}$$

Therefore, if the appearance of a peak is due to the weak-link behavior of a grain boundary, H_{peak} should be proportional to J_c^{Gr}. The peak fields versus the

corresponding companion grain current densities are shown in Figure 4-15. This figure shows a good linear dependency of H_{peak} on the companion grain current density J_c^{Gr}.

4.4 Results of the Low Field Study

In this section, we consider in more detail how currents are induced in the rings when small magnetic fields are applied, in other words, how the critical state is established. For the grain and 1.8° GB rings, magnetic moments were linearly dependent on the applied magnetic field up to the field range of 60~100 Oe, depending on sample conditions; see Figure 4-16-a. On the other hand, the linear dependence of $m(H)$ for the open rings continued up to approximately 200~250 Oe. After that, magnetic moments of open rings keep increasing up to the field of full penetration (~500 Oe), but sublinearly (Figure 4-16-b). As evident in Figure 4-16-b, the initial linear slopes of the open rings were much smaller than for grain samples. The difference in their slopes was due to their different geometry, by which the "pressure" applied on a sample by an external field was determined, i.e., the demagnetizing factors differ.

The properties of the GB ring samples in low fields were quite interesting. They showed a combination of the properties of grain and open rings. At very low fields, the GB ring samples resemble the grain ring samples (Figure 4-16-a). At that field range, magnetic moments of grain boundary samples increased linearly with same slopes of their companion grain rings, but this behavior did not continue. In small fields, around 7 Oe and 5 Oe for the 5.1° and 7° GB rings respectively, the magnetic moments began to

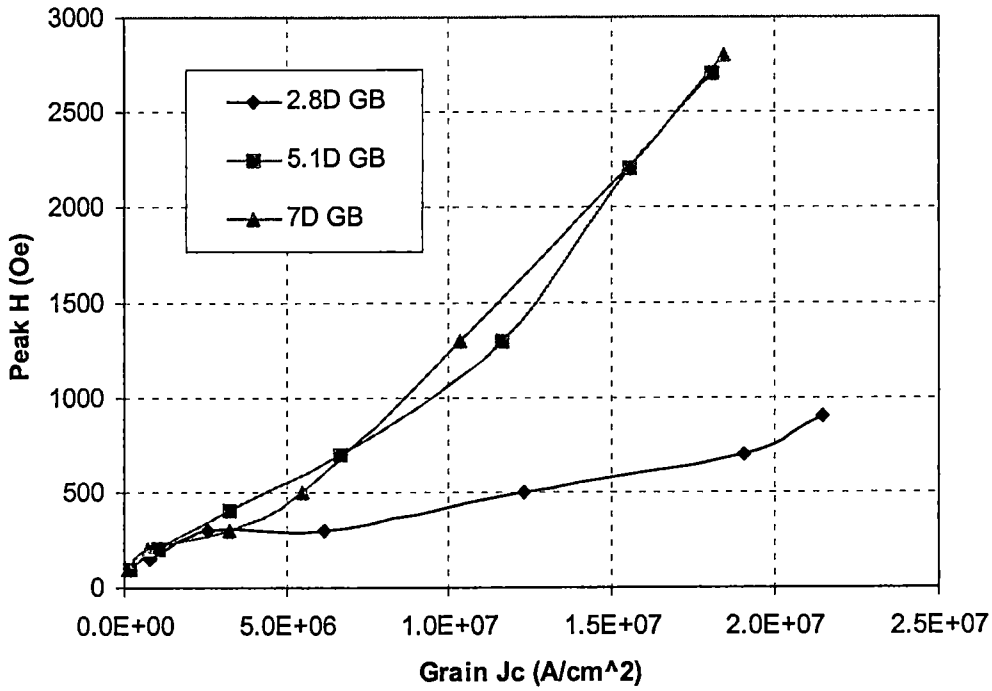

Figure 4-15. Peak field versus corresponding companion grain current density.

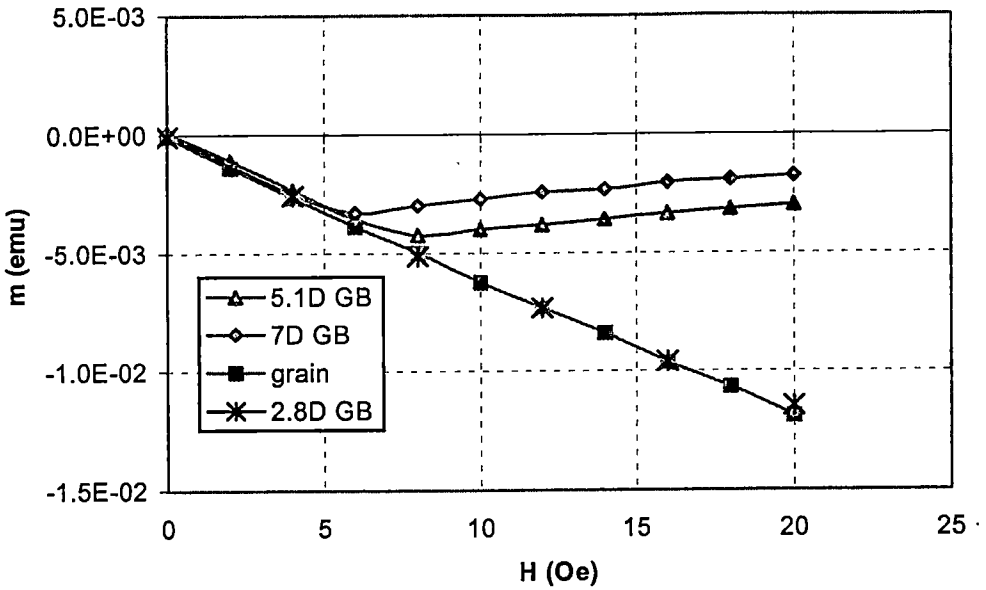

(a)

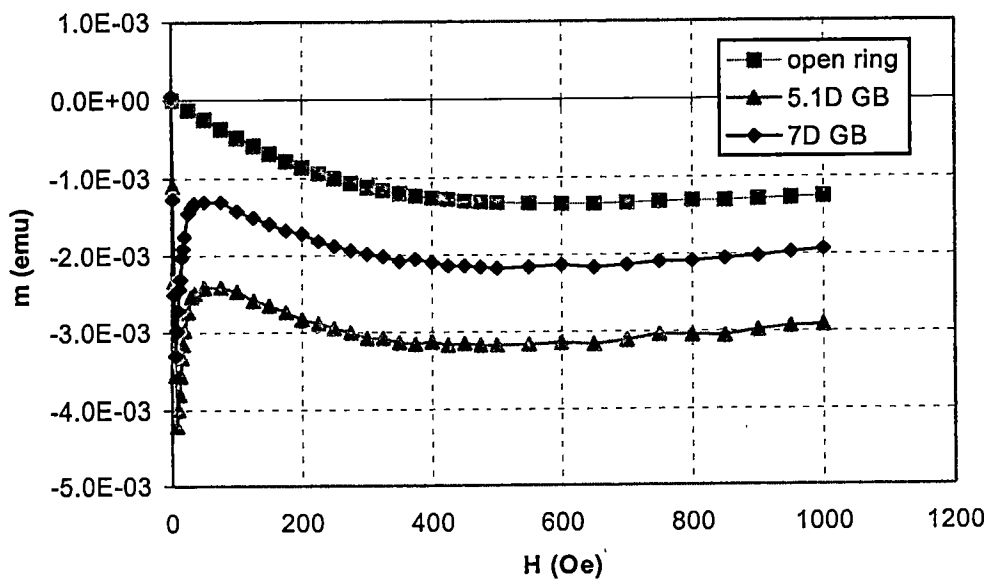

(b)

Figure 4-16. Magnetic moment versus field in the low field range: (a) grain, 2.8°, 5.1° and 7° GB rings, and (b) open, 5.1° and 7° GB rings.

decrease due to decreasing I_c in the grain boundary (Figure 4-16-a). At still higher applied fields near 50 Oe, the magnetic moments begin to increase again. Here the $m(H)$ curves strongly resemble those of open rings, but shifting down by a (roughly) constant amount. The shift corresponds to the magnetic moment created by the grain boundary current I_{GB} flowing around the ring of radius R. This open ring-like field dependency continues up to 65 kOe, the maximum field we applied.

At the fields in Figure 4-16-a where the linear dependency of magnetic moments of grain boundary samples ends (7 Oe and 5 Oe for 5.1° and 7° GB rings respectively), the entire 100 μm width of grain boundaries is conducting current and is fully penetrated by the magnetic field, whereas the grain areas were just partially penetrated by flux. Therefore, the magnetic field penetrates into the center of a GB ring when the applied field exceed those values. We explored this flux trapping process as follows. A small field (1,2,3,...Oe) was applied, the magnetic moments was measured, and then the field was reduced to zero. Each time after the magnetic moment of a ring sample was measured at a certain field, the field was removed and its zero field-induced magnetic moment was measured. Figure 4-17-b shows the result for a grain ring sample. Magnetic fields of ~ 60~70 Oe are needed to trap flux and to produce a non-zero value of zero field-induced magnetic moment. For the grain boundary samples, if less than a 7 Oe field for the 5.1° and 5 Oe for 7° GB ring was applied, a zero value of the zero field-magnetic moment was obtained (Figure 4-17-a). If the applied field exceeded those values, non-zero value of zero field-magnetic moment was measured. Therefore, at those fields, magnetic fields penetrated completely along the grain boundaries. The 2.8° GB ring sample also showed the same behavior and the onset of non-zero value of zero

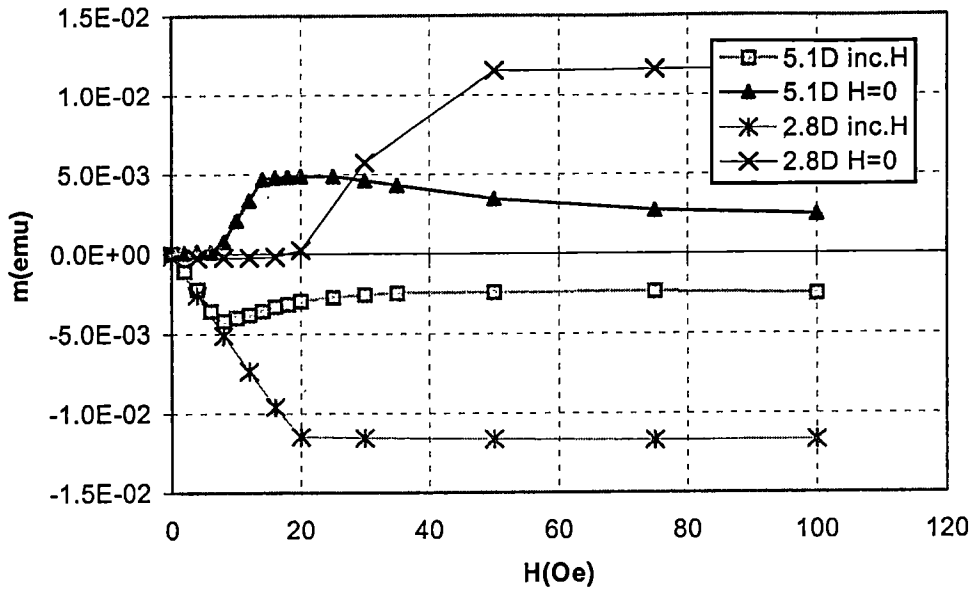

(a)

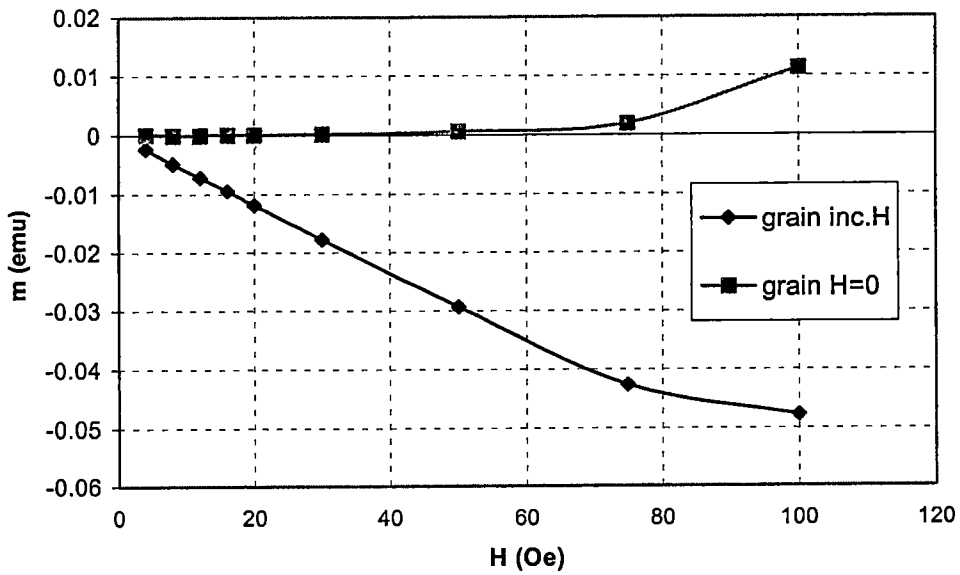

(b)

Figure 4-17. Magnetic moments at 5 K, showing in-field and trapped flux values, (a) for 2.8° and 5.1° GB ring. The symbols (×) and (▲) are values measured in H=0; they are plotted at values of H at which flux was trapped and (b) for a grain ring.

field-magnetic moment occurred at 20 Oe (Figure 4-17- a).

Interestingly, the slope of linearly increasing magnetic moments of a GB ring does not depend on temperature. Figure 4-18 shows the result of a small field study for a 5.1° GB ring sample at various temperatures. The slope is exactly same in all temperatures, but the fields where the linear dependency ends are different. This slope seems to depend on neither the angle of a grain boundary nor temperature. In fact, the situation corresponds simply to a Meissner-like state (B=0) inside the ring, while the slope is determined from the ring geometry through its effective demagnetizing factor.

4.5 Discussion

The temperature and field dependent study shows that a significant reduction of currents across grain boundaries occurs when the misorientation angle is greater than 1.8°. Furthermore, it was shown that the array of dislocation cores on a 1.8° grain boundary does not affect the critical current density at all. The critical current density values of the 1.8° GB ring samples were always very similar to those in the companion grain samples. This suggests that a 1.8° grain boundary either does not affect the grain boundary current density or it is overshadowed by some other property of the YBCO films. Indeed, the films on $SrTiO_3$ substrates contain a high density of twin boundaries, which are formed during the tetragonal-to-orthorhombic phase transition when synthesizing the YBCO thin films.[25] Along twin boundaries, the orthorhombic nature of the lattice is accommodated by a 1.8° misalignment of the $(1\bar{1}0)$ planes on either side of

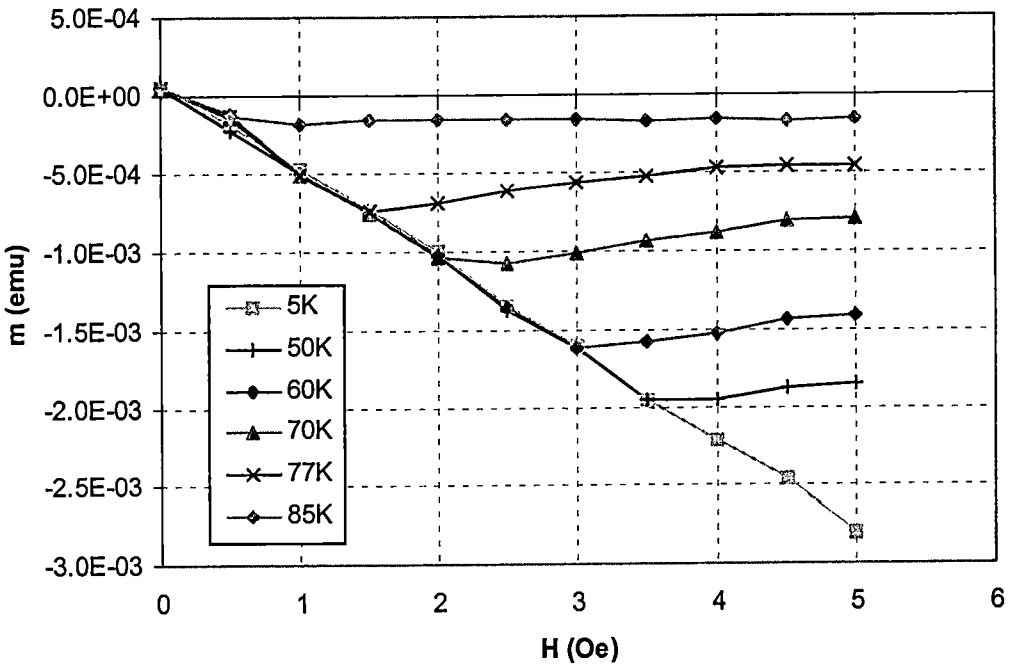

Figure 4-18. Magnetic moment versus field in the low field range for a 5.1° GB ring at various temperatures.

a (110) twin boundary.[26] In addition, dislocations called twinning dislocations are found in twin boundaries.[25] Therefore, a twin boundary may be somehow analogous to a 1.8° grain boundary. Consequently the grain part of the ring has a very large number of twin boundaries with accompanying 1.8° misorientations. While the twin boundaries do not contain dislocation cores, the presence of many 1.8° misorientations may mimic a 1.8° grain boundary. In other words, a grain ring effectively consists of a large number of 1.8° grain boundaries. Therefore, a 1.8° GB ring and its companion grain ring samples are indistinguishable in their current conduction.

Let us now consider the asymmetric curves of magnetic moment versus magnetic field curves for the 2.8°, 5.1°, and 7° GB ring samples, which contain peaks. These curves also give evidence for weak link behavior of a low angle grain boundary. We can simply assume that a low angle grain boundary consists of two parallel conduction regions, across one of which currents can flow and across the other of which just tunneling currents can flow (a weak link region or the Josephson junction). When fields are applied, a grain boundary is filled not only with applied fields penetrating into the sample but also with self fields created by currents flowing parallel to the sides of the grain boundary. Those two kinds of fields are in same direction when the applied field is increasing. It is already noted that the flow of tunneling current on a Josephson junction depends on the magnetic flux in the plane of the junction. Therefore, the total magnetic flux on each weak link region is large enough to severely reduce the tunneling current flowing across it in increasing field. In this case, large portions of currents are reflected at a grain boundary and must remain in the grain, creating strip-like magnetic moments. This view

of the in-field grain boundary explains why the field dependent $m(H)$ curves of GB rings appear similar to those of the open rings in increasing applied fields.

On the other hand, it should be noticed that in decreasing fields from 65 kOe to the peak fields, the features of the field dependent magnetic moment curves of the GB rings resemble those of grain rings. When the applied field is reduced from its maximum values of 65 kOe, induced currents begin to flow in opposite direction. In this case, the direction of the self field created by the induced currents on a grain boundary is opposed to that of applied fields and consequently the total magnetic flux on each weak link region at a certain applied field is relatively smaller than in the increasing applied fields case; for H increasing, $H_{total} \cong H_{app} + |H_{self}|$ and for H decreasing, $H_{total} \cong H_{app} - |H_{self}|$. As the applied field decreases, the grain current density and associated self-field becomes larger. In some field range, the total magnetic flux on a grain boundary become small enough to allow tunneling currents to flow through weak link regions. These tunneling currents become larger and larger, contributing to a growing ring-like moment. Therefore the characteristics of m versus H curves of GB ring samples in decreasing fields are similar to those of grain rings. For $H_{total} \approx 0$, the maximum grain boundary current density J_c^{GB} is obtained, this maximum J_c^{GB} creates the maximum magnetic moment, and this moment appears at the peak of the $m(H)$ curve of the GB ring.

A further decrease of the applied field leads to a rapid decrease of the magnetic moment. This decline may be explained by the fact that on a grain boundary, the self field produced by currents becomes larger than the applied field and the magnetic flux on the grain boundary begin to increase. As a result, the current across the grain boundary

decreases. The rapid decrease of magnetic moments after the peak field can be explained by the rapid increase of grain current densities as the applied field decreases.

The idea that the appearance of peaks on $m(H)$ curves of a GB ring sample is due to the weak link property of a grain boundary and a null H_{total} on the grain boundary is supported by the result of a following experiment using a 5.1° GB ring. After making a full $m(H)$ loop to 65 kOe, we then began to retrace the loop, increasing H from low field. Then at 2.2 kOe, the applied field was decreased in 20 Oe steps until the magnetic moment reached on the values on the decreasing field branch of the $m(H)$ curve (Figure 4-19). The changes were very gradual and a field change of at least 100 Oe was needed in order to reach the upper branch. This experiment was repeated by reversing the field sweep at 4 kOe, with similar results. On the other hand, when decreasing H from high fields to 2.6 kOe, an increase of H of 20 Oe produced a large reduction in the magnetic moment (see Figure 4-19). An increase of only 20 Oe from 2.6 kOe (which is the peak field of the 5.1° GB ring sample) or from 4 kOe is large enough to switch the magnetic moment almost to the increasing field branch, for both cases. Increasing the applied field from 1.8 kOe shows less diminution of a magnetic moment. It is suggested that near the peak field, while the field is decreasing, grain boundaries are very sensitive to field changes in the reverse direction. Those changes quickly add magnetic flux on the grain boundary; even a small field-increase changes the sign of H_{self} on a grain boundary, resulting in large changes in H_{total}. If the grain boundary is a weak link, then the tunneling current flowing across the grain boundary would drastically decrease upon even a very small change of magnetic flux on the grain boundary, just as this experiment shows.

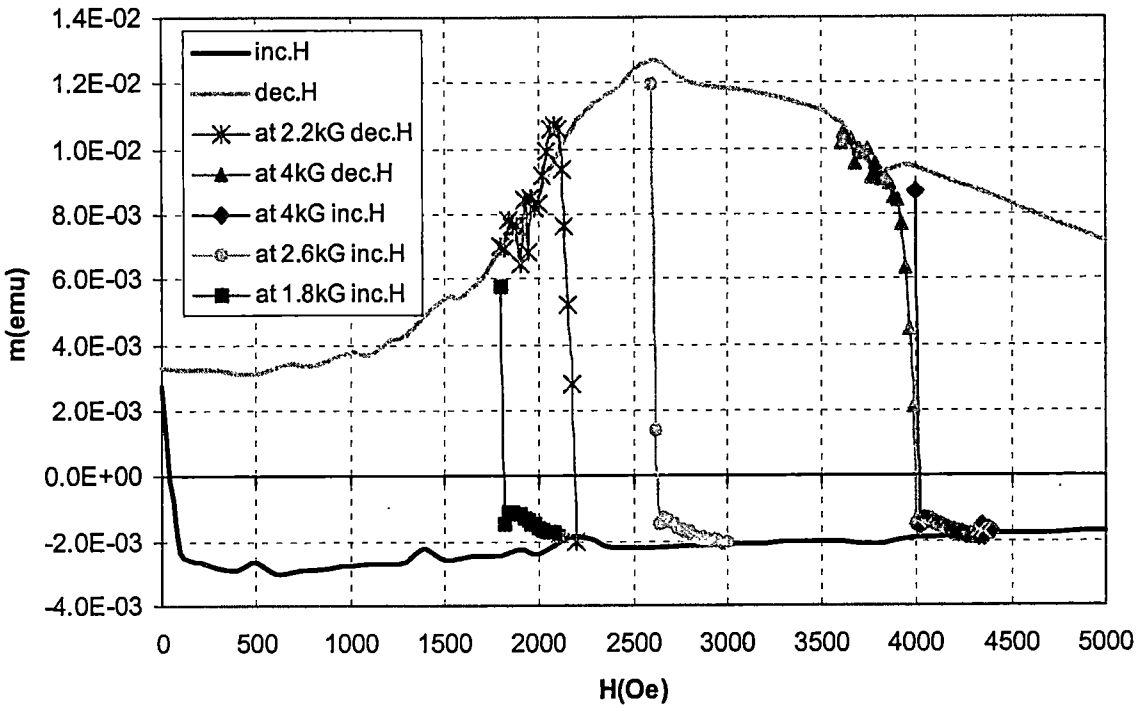

Figure 4-19. Magnetic moment changes due to applied field changes for a 5.1° GB ring at 5K; sudden decrease of an applied field from 2.2 kOe and 4 kOe during increasing field history (asterisks for 2.2 kOe and triangles for 4 kOe) and sudden increase of an applied field from 4 kOe, 2.6 kOe and 1.8 kOe during decreasing field history (diamonds for 4 kOe, circles for 2.6 kOe, and squares for 1.8 kOe).

CHAPTER 5

CONCLUSIONS

Taking advantage of the sensitivity of SQUID and the simple geometry of a sample that facilitates the calculation of a current in the sample, we have studied the current transport properties of small angle grain boundaries in YBCO thin films.

Relating the measured magnetic moments to the current configurations in GB, grain, and open ring samples, we could successfully separate the total magnetic moment of a GB ring into ring-like and strip-like moments, and obtain a pure grain boundary current density J_c^{GB}. This method was used to analyze the data from the temperature sweep experiment. Several properties of the small angle grain boundary were discovered in the temperature sweep experiment. First of all, even a very small misorientation on a YBCO thin film diminishes by a significant amount the grain boundary current density J_c^{GB}. The critical angle, at which a grain boundary begins to obstruct a current flowing across the grain boundary, seems to be in the range $1.8^\circ < \theta \leq 2.8^\circ$. Second, the current I_{GB} flowing across a small angle ($1.8^\circ \leq \theta \leq 7^\circ$) grain boundary subsists up to the grain critical temperature T_c. Finally, properties of 1.8° grain boundary are camouflaged by the large number of twin boundaries in a YBCO thin film, which form with 1.8° misalignments while synthesizing YBCO thin films on $SrTiO_3$ substrates; this is the reason why no difference between the 1.8° GB and its companion grain rings was observed.

From the low field study, we could see that even a small current created by the application of very small fields (few Oe) can not completely flow across a grain boundary; we observe some the current reflection at a grain boundary in very small fields. This directly shows that the current conducted by even a very small angle grain boundary ($1.8^\circ < \theta \leq 7^\circ$) is just the corresponding to a vortex distribution created by the low applied field (but enhanced by demagnetizing effects).

In the field sweep experiments, curves of magnetic moment versus field for the ring samples were obtained. Compared with the $m(H)$ curves of a grain or an open ring, the $m(H)$ curves of a GB ring shows several distinct properties. First of all, in increasing field, the $m(H)$ curve of a GB ring resembles that of an open ring, while in decreasing field, it is similar to that of a grain ring. Second, a huge peak appears on the $m(H)$ curve of a GB ring only in decreasing field. These two features of a $m(H)$ curve suggest that the current flowing across a grain boundary increases when the applied field decreases from its maximum value of 65 kOe. Furthermore, the peak field is proportional to the current density of a companion grain ring, measured at the same temperature and same field as the peak. Finally, in a decreasing field near the peak, even a small increase of the applied field changes the total magnetic moment by a huge amount; the grain boundary seems to be very sensitive to the total magnetic field on the grain boundary. All of those features can be explained by the weak-link behavior of a small angle grain boundary. This study clearly shows that a small angle grain boundary acts a weak-link, as does a large angle grain boundary.

In conclusion, this study suggests that to obtain the highest current density in YBCO thin films, and coated conductors with present grain boundary structures, it will

be necessary to reduce the grain boundary angle to around 1.8°. One conceptual approach is to design and operate the system so that the YBCO has zero total field on each grain boundary. Although very difficult (if not impossible) to implement, this would take advantage of the fact that the location of the peak is determined by the grain J_c, but does not depend on the grain boundary angle itself.

REFERENCES

REFERENCES

1. D. R. Tilley and J. Tilley, "*Superfluidity and Superconductivity*," Institute of Physics Publishing, Bristol and Philadelphia (1994).
2. A. Tonomura, "*The Quantum World Unveiled by Electron Waves*," World Scientific Publishing Co. (1998).
3. M. A. Omar, "*Elementary Solid State Physics*," Addison-Wesley publishing Co. (1993).
4. R. de Picciotto, H. L. Stormer, L. N. Pfeiffer, K. W. Baldwin, and K. W. West, Nature (London) **411**, 51 (2001).
5. Kyu Jeong Song, "*Superconducting Study of the Intermetallic* YNi_2B_2C *Crystal and Several High-*T_c *Materials*," Ph. D. Thesis, University of Tennessee (August, 1999).
6. G. Burns, "*High-Temperature Superconductivity*," Academic Press, Inc. (1992).
7. M. Imada, A. Fujimori, and Y. Tokura, Rev. Mod. Phys. **70**, 1039 (1998).
8. M. R. Beasley, IEEE Trans. Appl. Supercond. **5**, 141 (1995).
9. W. A. Little, Science **242**, 1390 (1988).
10. V. Z. Kresin, and S. A. Wolf, "*Fundamentals of Superconductivity*," Plenum Press, New York (1990).
11. Y. Yeshurun, A. P. Malozemoff, and A. Shaulov, Rev. Mod. Phys. **68**, 911 (1996).
12. J. R. Thompson, D. K. Christen, H. R. Kerchner, L. A. Boatner, B. C. Sales, B. C. Chakoumakos, H. Hsu, J. Brynestad, D. M. Kroeger, J. W. Williams, Y. R. Sun, Y. C. Kim, J. G. Ossandon, A. P. Malozemoff, L. Civale, A. D. Marwick, J. K. Worthington, L. Krusin-Elbaum, and F. Holtzberg in "*Magnetic Susceptibility of*

Superconductors and Other Spin System," edited by R. A. Hein, T. Francavilla, and D. Liebenburg (Plenum, New York, 1992), p. 157.

13. M. Tinkham, "*Introduction to superconductivity*" 2nd Ed., McGraw-Hill, New York (1995).
14. P. Chaudhari, J. Mannhart, D. Dimos, C. C. Tsuei, J. Chi, M. Oprysko, and M. Scheuermann, Phys. Rev. Lett. **60**, 1653 (1988).
15. J. Mannhart and H. Hilgenkamp, Mater. Sci. Eng. B **56**, 77 (1998).
16. M. F. Chisholm and D. A. Smith, Philos. Mag. 59, 181 (1989).
17. Y. Gao, K. L. Merkle, G. Bai, H. L. M. Chang, and D. J. Lam, Physica C **174**,1 (1991).
18. N. D. Browning, J. P. Buban, P. D. Nellist, D. P. Norton, M. F. Chisholm, and S. J. Pennycook, Physica C **294**, 183 (1998).
19. J. Mannhart and H. Hilgenkamp, Supercond. Sci. Technol. **10**, 880 (1997).
20. J. Mannhart, A. Kleinsasser, J. Strobel, and A. Baratoff, Physica C **216**, 401 (1993).
21. M. S. Chisholm and S. J. Penneycook, Nature (London) **351**,47 (1991).
22. H. Hilgenkamp, J. Mannhart, and B. Mayer, Phys. Rev. B **53**, 14586 (1996).
23. G. Hammerl, A. Schmehl, R. R. Schulz, B. Goetz, H. Bielefeldt, C. W. Schneider, H. Hilgenkamp, and J. Mannhart, Nature (London) **407**, 162 (2000).
24. A. Gurevich and E. A. Pashitskii, Phys. Rev. B **57**, 13878 (1998).
25. Y. Zhu and M. Suenaga in "*Interfaces in High-T_c Superconducting Systems*," edited by S. L. Shinde, and D. A. Rudman (Springer-Verlag, New York, 1994), p. 140.
26. D. T. Verebelyi, C. Cantoni, J. D. Budai, D. K. Christen, H. J. Kim, and J. R. Thompson, Appl. Phys. Lett. **78**, 2031 (2001).

VITA

Hyunjeong Kim was born in Seoul, Korea on March 8, 1974. She received her basic education in Hyo-Go, Japan and Seoul, Korea and graduated from Chung-Dam high school in February 1993. The following March, she entered Sejong University, in Seoul, Korea and received a Bachelor of Science degree in Physics in February 1997. In September 1998, she began her graduate studies toward a Master of Science degree in physics at the University of Tennessee, Knoxville and accepted a teaching assistantship in January of 1999. She expects to receive the Master of Science degree in December of 2001.

Hyunjeong Kim is a member of Sigma Pi Sigma Physics Honor Society and the American Physical Society.